tem (Promega) using a 2030 ARVO X luminometer (PerkinElmer) according to the manufacturer's instructions.

Immunofluorescence microscopy. Cells were fixed with 3% paraformaldehyde for 10 min at room temperature and then blocked with 0.1% Triton–3% FCS–HBS (21 mM HEPES buffer [pH 7.4], 1.8 mM disodium hydrogen phosphate, 137 mM NaCl, 4.8 mM KCl). The cells were stained by indirect immunofluorescence with primary antibodies against FLAG (mouse antibody 2H8; TransGenic Inc.), VCP (mouse and rabbit antibody; Abcam), GBF1 (mouse antibody [BD Transduction Laboratory] and rabbit antibody [Abcam]), PI4KB (mouse antibody [BD Transduction Laboratory] and rabbit antibody [Millipore]), double-stranded RNA ([dsRNA] English & Scientific Consulting Bt), PV 3A (rabbit antibody), PV 3B (rabbit antibody), secondary antibodies (anti-mouse or anti-rabbit goat antibodies conjugated with Alexa Fluor 488, 594, and 350 dyes [Molecular Probes]), and Hoechst 33342 (Molecular Probes) for counterstaining of nuclei (2). For double staining of GBF1 and 3A, cells were blocked with anti-rabbit goat serum (Jackson ImmunoResearch) after GBF1 staining and before staining against 3A protein. For labeling of nascent viral RNA, PV-infected cells were treated with 10 μg/ml of actinomycin D at 3 h postinfection (p.i.) for 1 h and then were transfected with bromouridine triphosphate (BrUTP) by using *Trans*IT-293 transfection reagent (Mirus). The cells were incubated at 37°C for 20 min and then stained with anti-bromodeoxyuridine antibody (Roche), followed by anti-mouse goat antibodies conjugated with Alexa Fluor 594 (Molecular Probes). Samples were observed with a confocal scanning laser microscope (FV1000; Olympus).

Immunoprecipitation. pKS435-3AB-His, -2BC-His, and -2C-His, with FLAG-VCP, VCP-GFP-FLAG, or VCP-GFP (without the FLAG tag), expression vectors were transfected into HEK293 cells cultured on a six-well plate using Lipofectamine 2000 (Invitrogen) according to the manufacturer's instruction. At 48 h p.t., cells were washed twice with DMEM, and then cytosolic protein fractions were prepared by using a Proteo-Extract Transmembrane Protein Extraction Kit (Novagen). Cytosolic protein fractions were mixed with 20 μl of prewashed anti-FLAG magnetic beads (anti-FLAG M2 magnetic beads; Sigma-Aldrich) and then incubated for 1 h on a rotator at 4°C. The beads were washed three times with washing buffer (20 mM HEPES [pH 7.4], 137 mM NaCl, 1.8 mM $MgCl_2$) and then boiled in SDS-PAGE sample buffer. Samples were subjected to Western blot analysis with anti-His tag antibody (Penta-His HRP Conjugate; Qiagen) (for detection of 3AB-His, 2BC-His, and 2C-His) and anti-VCP antibody (for detection of FLAG-tagged VCPs and endogenous VCP).

Western blot analysis. Samples were subjected to 5 to 20% gradient polyacrylamide gel electrophoresis (e-PAGEL; Atto Corporation) in a Laemmli buffer system (57). The proteins in the gel were transferred to a polyvinylidene difluoride filter (Immobilon; Millipore) and blocked by using a blocking reagent (Qiagen). The filters were incubated with anti-His tag antibody (Penta-His HRP Conjugate; Qiagen), anti-FLAG tag antibody (anti-FLAG M2-peroxidase antibody; Sigma-Aldrich), and mouse anti-VCP antibody (Abcam) (at 1:1,000, 1:300, and 1:3,000) in a SNAP i.d. System (Millipore). The filters were washed with phosphate-buffered saline ([PBS] 10 mM phosphate buffer [pH 7.0], 135 mM NaCl, and 2.6 mM KCl) containing 0.1% Tween 20 (PBS-T) three times. For detection with anti-VCP antibody, the filters were incubated with goat anti-rabbit IgG antibodies conjugated with horseradish peroxidase ([HRP] 1:1,000 dilution; Pierce). The filters were washed by PBS-T three times and then treated with SuperSignal West Femto Maximum Sensitivity Substrate (Pierce) for the detection of the signal.

Mammalian two-hybrid assays. The mammalian two-hybrid assays were performed as described previously using a Checkmate mammalian two-hybrid system (Promega) (46, 85). VCP and PV proteins (2B, 2BC, 2C, 3A, and 3AB) were expressed as fusion proteins in pFN10A(ACT) Flexi vector (pACT-VCP, PV-2B, PV-2BC, PV-2C, PV-3A, and PV-3AB) and pFN10A(BIND) Flexi vector (pBIND-VCP, PV-2B, PV-2BC, PV-2C, PV-3A, and PV-3AB). pACT-VCP and pBIND-VCP were cotransfected with pBIND-PV protein expression vectors and pACT-PV protein expression vectors, respectively, with a reporter plasmid (pGL4.31[luc2P/GAL4 UAS/Hygro]) into HEK293 cells. pACT and pBIND empty vectors were used with pBIND-VCP and pACT-VCP as controls, respectively. Firefly luciferase activity (derived from a reporter plasmid produced by binding of fusion proteins) and *Renilla* luciferase activity (derived from pBIND vectors for normalization of transfection efficiency) were measured at 24 h p.t. of DNA. The ratio of firefly luciferase to *Renilla* luciferase was calculated and then normalized by the ratio of the controls.

PLA. A proximity ligation assay (PLA) was performed by using Duolink II reagents (Olink Bioscience). HEK293 cells expressing 3AB or 2BC proteins were fixed and permeabilized as described in indirect immunofluorescence and then incubated with antibodies. For detection of PLA signals, anti-3B or -2C antibodies (rabbit antibodies) were used with anti-VCP antibody (mouse antibody) (for detecting PLA signal between 3AB/2BC and VCP), and the individual antibody (anti-3B, -2C or -VCP antibody) was used as a negative control in the PLA. After the PLA, cells were subjected to indirect immunofluorescence to detect 3AB, 2BC, and VCP in the cells with secondary antibodies (anti-rabbit or anti-mouse goat antibodies conjugated with Alexa Fluor 488). Samples were observed with a confocal scanning laser microscope (FV1000; Olympus).

Isolation of PV mutants resistant to VCP knockdown. VCP siRNA-transfected HEK293 cells in 96-well plates were infected with PV1 (Mahoney) at a multiplicity of infection (MOI) of 10 or 1 at 72 h p.t. of VCP siRNA. The cells were incubated at 37°C and then collected at day 2 p.i. Collected cell lysates were mixed and then used for the next passage. The resistance phenotype of the virus was observed by the appearance of cytopathic effect (CPE) after four passages. Resistant mutants were isolated by limiting dilution, and then the structural and nonstructural protein-encoding regions of the viral genomes were analyzed as previously described (8).

***Gaussia* luciferase secretion assay.** VCP-, GBF1-, and PI4KB-siRNA- or mock-transfected HEK293 cells in 96-well plates were transfected with 0.2 μg per well of expression vectors encoding PV 2B, 2BC, 3A, and 3AB or EGFP (control vector) and 0.002 μg per well of pTK-Gluc vector encoding *Gaussia* luciferase by using a Lipofectamine 2000 reagent (Invitrogen) at 48 h p.t. of siRNA. Supernatants of transfected cells were collected at 20 h p.t. of DNA, and then the luciferase activity in the supernatants was measured with a BioLux *Gaussia* Luciferase Assay kit (New England BioLabs, Inc.) using a 2030 ARVO X luminometer (PerkinElmer) according to the manufacturer's instructions.

Statistical analysis. The results of experiments are shown as the averages with standard deviations. The effect of siRNA treatment on PV infection was analyzed by a *t* test. *P* values of less than 0.05 were considered significant and are indicated by asterisks in the figures.

RESULTS

siRNA screening targeting membrane-trafficking genes for host factors required for PV replication. We performed screening with an siRNA library targeting 140 membrane-trafficking genes for host factors required for PV infection by using a PV pseudovirus infection system (4, 7). A summary of the results of the screening is shown in Fig. 1A and in Table S1 in the supplemental material. The mean and median net PV pseudovirus infection values of the siRNA screening were 1.9, and 1.7, respectively. siRNA targeting VCP showed the highest inhibitory effect on PV pseudovirus infection (net PV pseudovirus infection of 0.0036) among the examined siRNAs (Fig. 1B). An interferon (IFN) response, which could be induced by siRNA treatment (78), was not observed in the cells treated with an siRNA targeting VCP (Fig. 1C). We analyzed the inhibitory effect of an siRNA targeting VCP, along with one that targets a PV host factor, GBF1 (91), on PV infection (Fig. 1D). The copy number of viral RNA of PV1 (Mahoney) in the cells treated with an siRNA targeting VCP was about

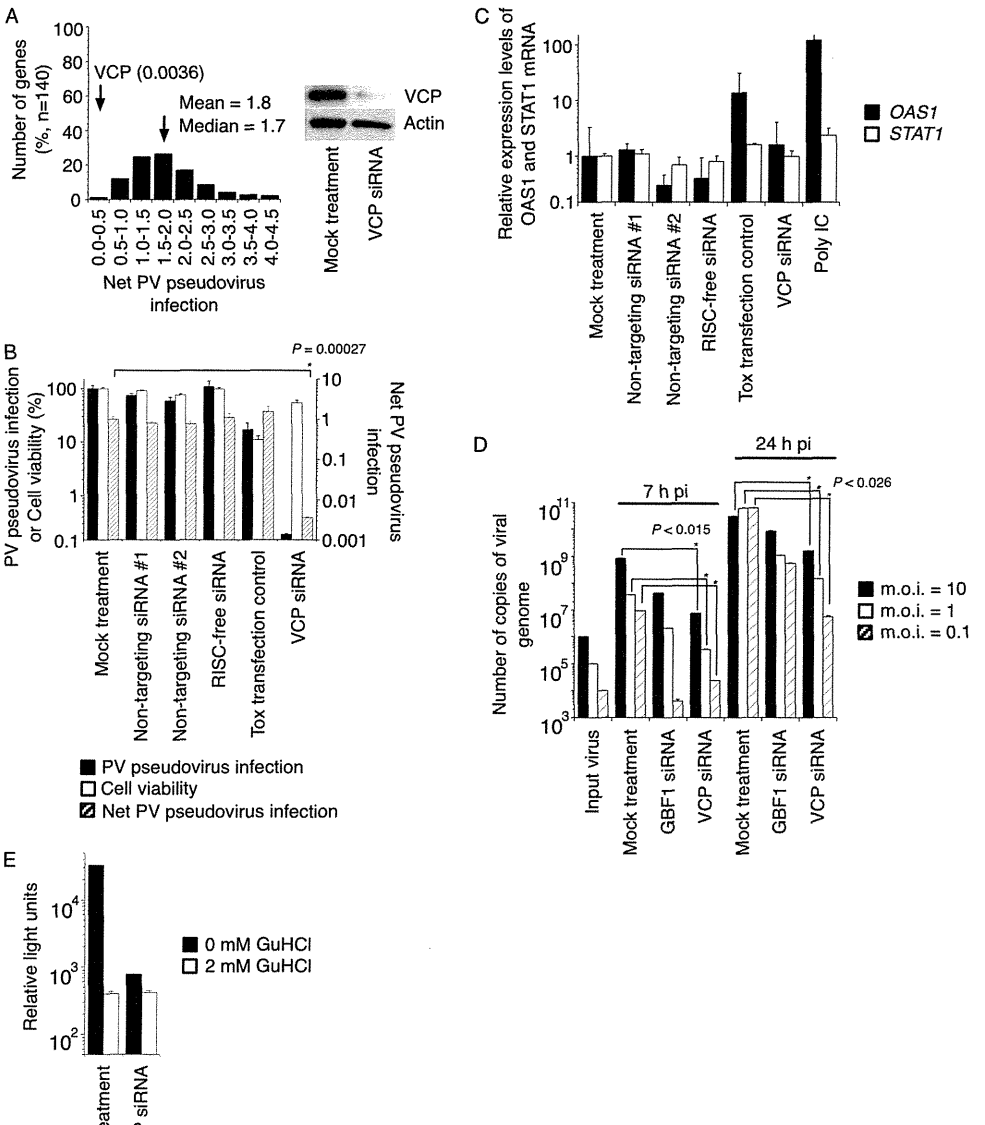

FIG 1 Screening of an siRNA library targeting membrane-trafficking genes for host factors of PV infection. (A) Screening of an siRNA library targeting membrane-trafficking genes. The left panel shows distribution of net PV pseudovirus infection values of siRNAs targeting 140 genes. The distribution of the numbers of genes in each range of net PV infection values is shown. Cells transfected with VCP-siRNAs showed the highest inhibitory effect on PV pseudovirus infection (0.0036 of net PV pseudovirus infection). The right panel shows Western blot analysis of VCP expression in cells treated with VCP-siRNA. (B) Inhibitory effect of VCP-siRNA treatment on PV pseudovirus infection. PV pseudovirus infection, cell viability, and net PV pseudovirus infection in siRNA-transfected cells are shown. (C) Interferon response to siRNA treatment. Expression levels of mRNAs of OAS1 and STAT1 in siRNA-transfected cells are shown. (D) Inhibitory effect of siRNA treatment targeting VCP and GBF1 on PV1 (Mahoney) infection. Cells were infected with PV1 (Mahoney) at an MOI of 10, 1, or 0.1, and then the amounts of viral genome in the cells were analyzed at 7 or 24 h p.i. Numbers of copies of viral genome of input virus and in infected cells are shown. (E) Viral protein synthesis in VCP-knockdown cells. Mock- and VCP-siRNA-treated cells (1.0×10^4 cells) were infected with PV pseudovirus (6.5×10^5 IU) in the presence (2 mM) or absence of GuHCl. Luciferase activities in the cells at 2 h p.i. are shown.

1/100 of that in mock-treated cells at 7 h p.i., suggesting a high inhibitory effect of the siRNA targeting VCP as well as that of the siRNA targeting GBF1. Viral protein synthesis in VCP-siRNA-treated cells was measured in the presence of the PV replication inhibitor GuHCl. The level of viral protein synthesis in VCP-siRNA-treated cells was similar to that in mock-treated cells in the presence of GuHCl (Fig. 1E). These results suggested that VCP is a host factor for PV replication required after viral protein synthesis.

VCP colocalizes with viral 2BC/2C and 3AB/3B proteins and interacts with 2BC and 3AB proteins. To analyze involvement of VCP in PV replication, we analyzed colocalization of VCP with viral proteins in PV-infected cells. We analyzed colocalization of VCP with viral proteins 2BC/2C, 3A/3AB, 3AB/3B, double-stranded RNA (dsRNA), and nascent viral RNA (Fig. 2). VCP was observed in both the nucleus and cytoplasm of mock-infected cells (65) and showed a partial accumulation in the cytoplasm after PV infection (data not shown). In high-resolution images, VCP ap-

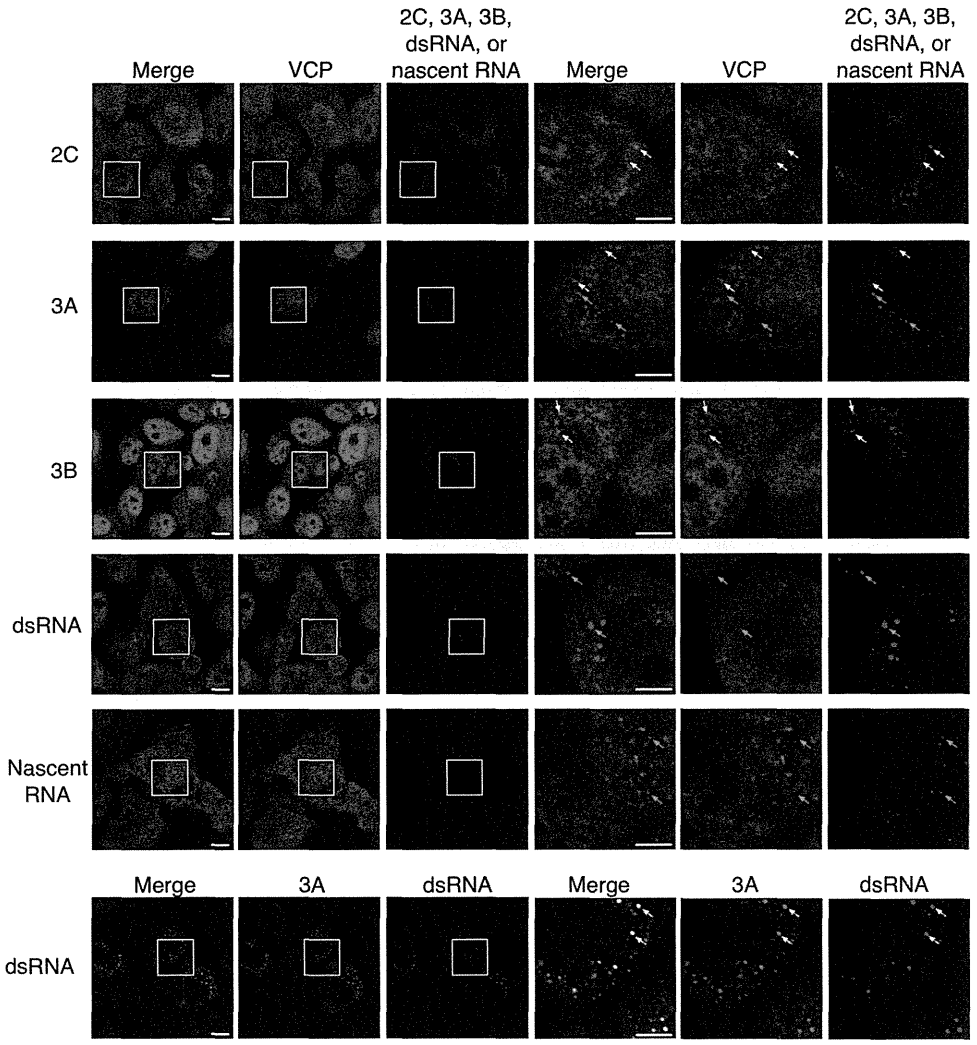

FIG 2 Localization of viral proteins, viral RNAs, and VCP in PV-infected RD cells. The first five rows show indirect immunofluorescence of viral proteins 2C, 3A, 3B, dsRNA, and VCP (nascent RNA) in PV-infected cells at 4 h p.i. The three right-most columns show magnified views of the boxed areas in the first three columns. Blue, nucleus (staining with Hoechst 33342); green, VCP; red, 2C, 3A, 3B, dsRNA, or nascent viral RNA. Scale bars, 10 μm (first three columns) and 5 μm (three right-most columns). The bottom row shows indirect immunofluorescence images of viral proteins 3A and dsRNA in PV-infected cells. The columns are as described above. Blue, nucleus (staining with Hoechst 33342); green, 3A; red, dsRNA. Scale bars, 10 μm (first three panels) and 5 μm (three right-most panels). White arrows indicate some of the colocalized sites, and cyan arrows indicate some of the noncolocalized sites.

peared as a small dot-like structure in PV-infected cells and colocalized with viral proteins 2BC/2C and 3AB/3B. 3A and dsRNA colocalized in PV-infected cells but not with VCP. VCP also did not show colocalization with nascent viral RNA. We also analyzed localization of PI4KB and GBF1 in PV-infected cells (Fig. 3). 2BC/2C and 3AB/3B colocalized with PI4KB and GBF1; however, colocalization of dsRNA was observed only with PI4KB and not with GBF1 and VCP.

Next, we analyzed localization of VCP in cells transiently overexpressing individual viral proteins 2BC, 2C, 3A, and 3AB (Fig. 4A). VCP showed complete colocalization with 2BC and 3AB and partial colocalization with 2C and 3A. Overexpression of 3A caused drastic relocalization of VCP in the cytoplasm to form vesicle-like structures, previously observed as swelling of endoplasmic reticulum (ER) in 3A-expressing cells (33), but only partial colocalization with VCP was observed. 3AB localized in perinuclear regions of transfected cells, consistent with a previous observation (29), and showed complete colocalization with VCP. To determine the region of 3AB responsible for VCP interaction, we analyzed colocalization of VCP with deletion mutants of 3AB. We found that the deletion mutant 3A(Δ1–41)B, which lacks aa 1 to 41 of 3A including residues involved in 3A dimerization (aa 25 to 43) (81), appeared as a small dot-like structure in the cytoplasm and colocalized with VCP. GBF1 and PI4KB colocalized with 3AB and VCP but not with the deletion mutant 3A(Δ1–41)B (data not shown).

We analyzed the interaction of VCP with viral proteins by a mammalian two-hybrid assay (Fig. 4B). We found that only 2BC and not 2B, 2C, 3A, or 3AB showed an interaction with VCP in this assay. The interaction of VCP with 3AB and 2BC, but not with 2C, was detected by immunoprecipitation (Fig. 4C), and the proximity of 3AB/2BC and VCP was detected by PLA (79) (Fig. 4D). This suggested that VCP interacts with viral proteins 2BC and 3AB by a mode that differs from that of GBF1 and PI4KB.

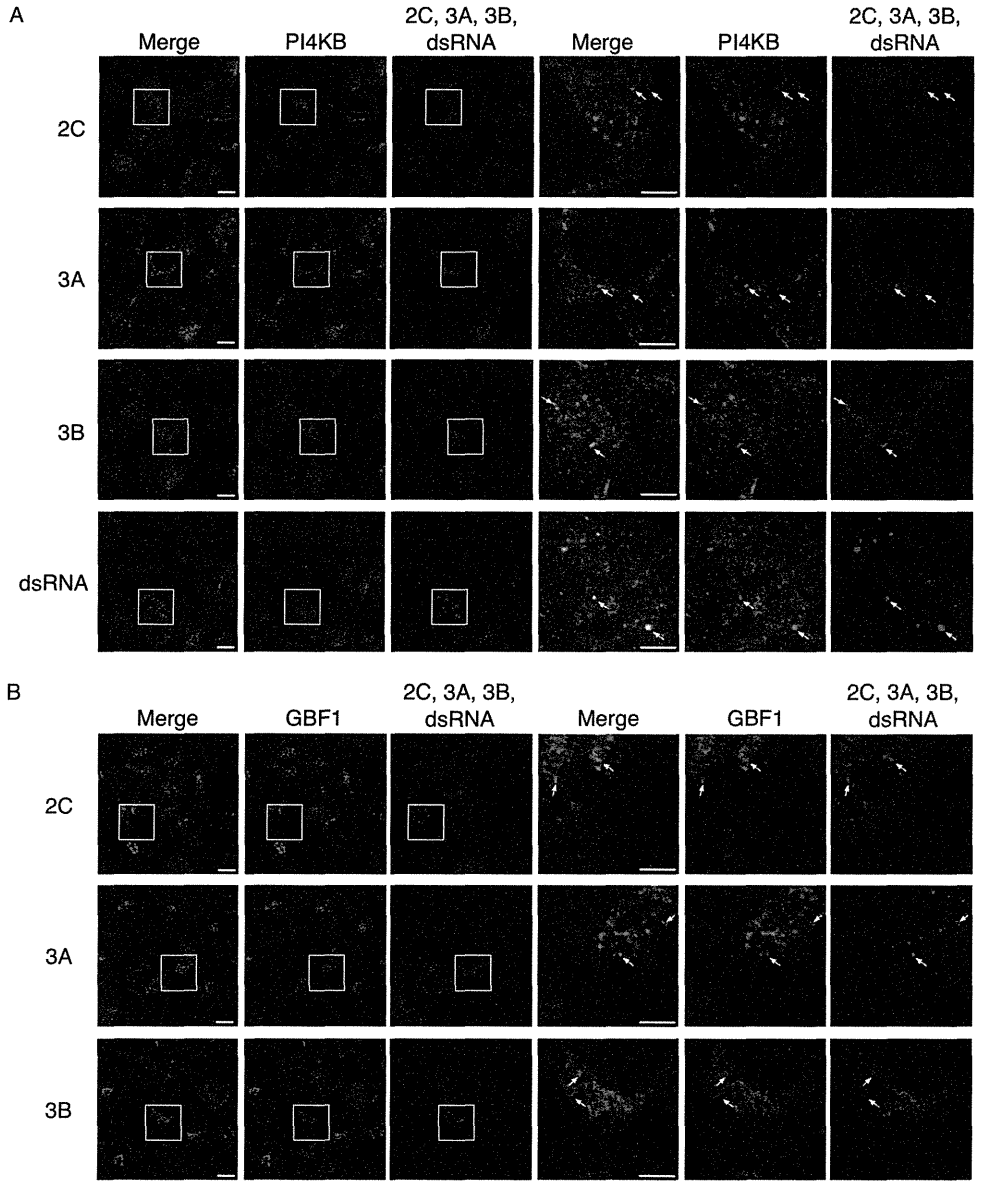

FIG 3 Localization of viral proteins, viral RNAs, and PI4KB and GBF1 in PV-infected RD cells. Indirect immunofluorescence images of PI4KB (A) or GBF1 (B) are shown. The three right-most columns are magnified views of the boxed areas in the first three columns. Blue, nucleus (staining with Hoechst 33342); green, PI4KB or GBF1; red, 2C, 3A, 3B, or dsRNA. Scale bars, 10 μm (first three columns) and 5 μm (three right-most columns). White arrows indicate some of the colocalized sites, and cyan arrows indicated some of the noncolocalized sites.

ATPase activity of VCP is essential for PV replication. To determine the importance of the biological function of VCP in PV replication, we analyzed VCP mutants with different levels of ATPase activities; two mutants with increased ATPase activity [VCP(A232E) and VCP(R191Q)] (38, 59) and a mutant deficient in ATPase activity [VCP(K524A)] (55) were used. The transfection efficiency of VCP mutants was more than 80% as observed by EGFP tag expression; however, expression of none of the VCP mutants affected PV replicon replication (Fig. 5). This suggested that a dominant negative effect of VCP(K524A) was not observed in PV infection. We reasoned that endogenous VCP, which is an abundant ATPase comprising 14% of the amount of actin or 0.7% of total cytoplasmic proteins (65), might serve as a host factor for PV replication even in the presence of a dominant negative VCP mutant. Therefore, we analyzed the effect of VCP mutants on PV replication in cells depleted of endogenous VCP with an siRNA treatment targeting VCP. VCP mutants used for expression experiments were derived from a mouse VCP orthologue (59), which

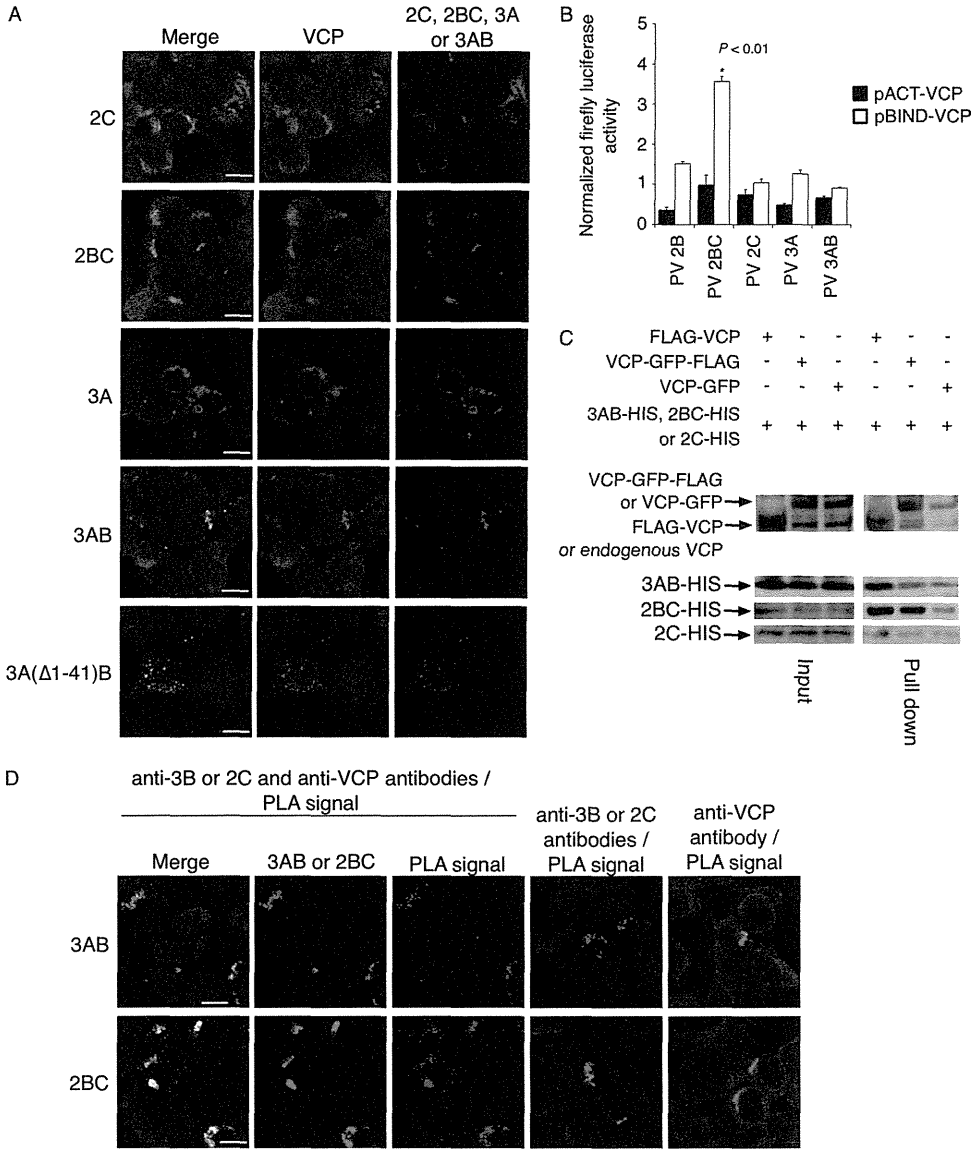

FIG 4 Localization of overexpressed viral proteins with VCP. (A) Localization of VCP in HEK293 cells expressing 2C, 2BC, 3A, and 3AB mutants. Blue, nucleus (staining with Hoechst 33342); green, VCP; red, 2C, 2BC, 3A, 3AB, or a 3AB mutant. Scale bar, 10 μm. (B) Mammalian two-hybrid assay for VCP and PV proteins. Closed bars, pACT-VCP and pBIND-PV proteins; open bars, pBIND-VCP and pACT-PV proteins. Normalized firefly luciferase activities are shown. (C) Immunoprecipitation of 3AB, 2BC, and 2C with VCP. HEK293 cells expressing 3AB, 2BC, or 2C (3AB-His, 2BC-His, or 2C-His) with FLAG-VCP, VCP-GFP-FLAG, or VCP-GFP were precipitated by anti-FLAG antibody. The amounts of VCP and viral proteins in input (4% of cell lysate used for immunoprecipitation) and pulldowns (immunoprecipitated with anti-FLAG antibody) were analyzed by Western blotting with anti-VCP antibody (for FLAG-VCP, VCP-GFP-FLAG, and VCP-GFP) or anti-Penta-His antibody (for 3AB-His, 2BC-His, and 2C-His). (D) PLA signals between viral proteins and VCP in 3AB- and 2BC-expressing cells. 3AB- and 2BC-expressing cells were incubated with anti-3B/2C antibodies with anti-VCP antibody (left six panels) or with individual antibodies (anti-3B/2C antibodies or anti-VCP antibody) and then subjected to PLA. Blue, nucleus (staining with 4′,6′-diamidino-2-phenylindole[DAPI]); green; 3AB or 2BC or VCP; red, PLA signals.

has 100% amino acid similarity to human VCP but is resistant to an siRNA targeting human VCP, for mutations in the target sites of the siRNA. In VCP-knockdown cells, only VCP mutants with ATPase activity rescued PV replication (Fig. 5). This suggested that the ATPase activity of VCP is essential for PV replication irrespective of the levels of ATPase activity and that the inhibitory effect of VCP-siRNA on PV replication was caused by the depletion of VCP and not by the off-target effect of siRNA.

Knockdown of VCP suppressed PV infection but not CVB3 infection and enhanced AV replication. To analyze the effect of VCP knockdown on the replication of picornavirus, we first analyzed AV replication in VCP-knockdown cells (Fig. 6). AV is a member of the genus *Kobuvirus* of the family *Picornaviridae* (97). Knockdown of VCP significantly suppressed replication of the PV replicon but enhanced the replication of the AV replicon (about a 9-fold increase) (Fig. 6A). Next, we analyzed the infection of CVB3, which belongs to another EV species, *Human enterovirus B*, in VCP-knockdown cells (Fig. 6B). The titers of type 1, 2, and 3 PV (Sabin), but not of CVB3, were reduced in VCP-knockdown cells at both 7 h p.i. and 24 h p.i. These results suggested that the effect

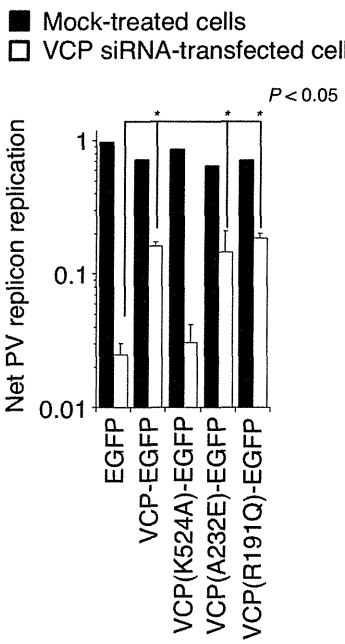

FIG 5 Role of ATPase activity of VCP in PV replication. PV replicon replication was analyzed in mock-treated and VCP-siRNA-transfected HEK293 cells expressing EGFP (control) or VCP mutants. A *t* test was performed for the net PV replicon replication between EGFP-expressing cells (control) and cells expressing each of the VCP mutants.

of VCP knockdown on viral replication is different among members of the picornavirus family.

VCP acts as a host factor of PV replication via a cellular secretion pathway. Next, we attempted to isolate a resistant PV mutant that could show efficient infection in VCP-knockdown cells. We repeated passage of PV1 (Mahoney) in VCP-knockdown cells, and we observed a clear CPE in the infected cells after five passages, in contrast to inapparent and delayed CPE in parental PV1 (Mahoney)-infected cells. An isolated resistant clone showed improved growth in VCP-knockdown cells compared to the parental PV1 (Mahoney) strain (Fig. 6C, right panel). This clone had only one amino acid change in the viral proteins, a 2C-E253G mutation, which is known as the determinant of a PV mutant for a secretion inhibition-negative phenotype (19). Sequences of 2C around aa 253 are not conserved in picornaviruses but are conserved among PV strains. PV pseudovirus with an A4881G (2C-E253G) mutation showed a resistance phenotype in VCP-knockdown cells (Fig. 6D). The resistance phenotype is stronger in cells treated with VCP-siRNA for 48 h than that in cells treated for 72 h, suggesting that PV with a 2C-E253G mutation retained dependency on VCP for its replication. The effect of the 2C-E253G mutation on 2BC binding to VCP was evaluated with a mammalian two-hybrid assay (Fig. 6E). Consistent with the above observation, increased luciferase signals were detected for 2BC with a 2C-E253G mutation [2BC(2C-E253G)] with VCP, suggesting an increased affinity between 2BC and VCP by this mutation. These results suggested that VCP acts as a host factor of PV replication, possibly via a cellular secretion pathway.

VCP is not required for inhibition of cellular protein secretion caused by overexpression of individual viral proteins. To analyze the role of VCP in inhibition of cellular protein secretion by PV infection, we examined cellular protein secretion in VCP-siRNA-treated cells expressing each of the viral proteins 2B, 2BC, 3A, and 3AB (Fig. 7). We observed strong inhibition of the secretion of *Gaussia* luciferase caused by overexpression of 2B, 2BC, and 3A, consistent with a previous report (34), and also a weak inhibitory effect of 3AB. In PI4KB- and VCP-siRNA-treated cells, suppression of the inhibitory effect caused by viral proteins, including 2B, 2BC, 3A, and 3AB, was observed; however, the apparent inhibitory effect of each individual viral protein in this *in vitro* system depended on the transfection efficiency of DNA that was evaluated by *Gaussia* luciferase activity in the cell supernatants and by *Renilla* luciferase activity in the cells (Fig. 7A, right panel). The PI4KB- and VCP-siRNA treatments significantly reduced the DNA transfection efficiencies in the treated cells, and specific suppression effects beyond the reduced DNA transfection efficiency were not observed. In contrast, GBF1 knockdown enhanced the inhibitory effect of 3AB. We also analyzed the effect of a 2C-E253G mutation on the inhibitory effect of 2BC but could not detect a significant suppression of the inhibitory effect caused by 2BC with a 2C-E253G mutation (Fig. 7B). These results suggested that VCP did not suppress the inhibition of cellular protein secretion caused by overexpression of each individual viral protein.

DISCUSSION

In this study, we identified VCP as a host factor required for PV replication by siRNA screening targeting membrane-trafficking genes. Important host factors involved in virus replication have been identified in this pathway of genes, including PI4KA, which showed the highest inhibitory effect on hepatitis C virus (HCV) replication in siRNA screening (14). VCP was originally identified as the protein that contains the amino acids of valosin peptide, which was considered a physiologically active peptide but turned out to be an artifact by the analysis of amino acid sequence of VCP (56). Analysis of VCP showed that VCP belongs to the class I AAA+ family (92) and has roles in a variety of cellular processes, including protein degradation pathways (64, 69, 95), homotypic membrane fusions (i.e., Golgi reassembly [68], transitional ER reassembly [71], and nuclear envelope assembly [41]). Mutations of VCP cause a dominantly inherited disorder, inclusion body myopathy associated with Paget disease of bone and frontotemporal dementia (IBMPFD) (76, 88), possibly by interfering with the ubiquitin-dependent protein degradation pathway (e.g., immature autophagosome formation) (50, 52, 87) by enhancing ATPase activity of VCP (38, 59). In PV replication, VCP targeted the replication step after viral protein synthesis, and ATPase activity of VCP was essential irrespective of the levels of activity of the VCP mutants examined (Fig. 1E and 5). VCP mutants with IBMPFD mutations or with an ATPase activity-deficient mutation (K524A) are known to interfere with clearance of ubiquitinated proteins because of impaired aggresome formation (51, 53, 54, 89, 90, 96). Our observations suggested that some level of ATPase activity of VCP is sufficient to support PV replication and that fine-tuned ATPase activity required for normal ubiquitin-dependent protein degradation is not necessary for PV replication.

In PV-infected cells, VCP colocalized with viral proteins 2BC/2C and 3AB/3B but not with 3A, dsRNA, or nascent viral RNA (Fig. 2). 2BC/2C and 3AB/3B also colocalized with PI4KB and GBF1 in PV-infected cells (Fig. 3). However, colocalization of dsRNA was observed only with PI4KB and not with GBF1 and VCP. This may suggest a functional difference of these 3A/3AB-

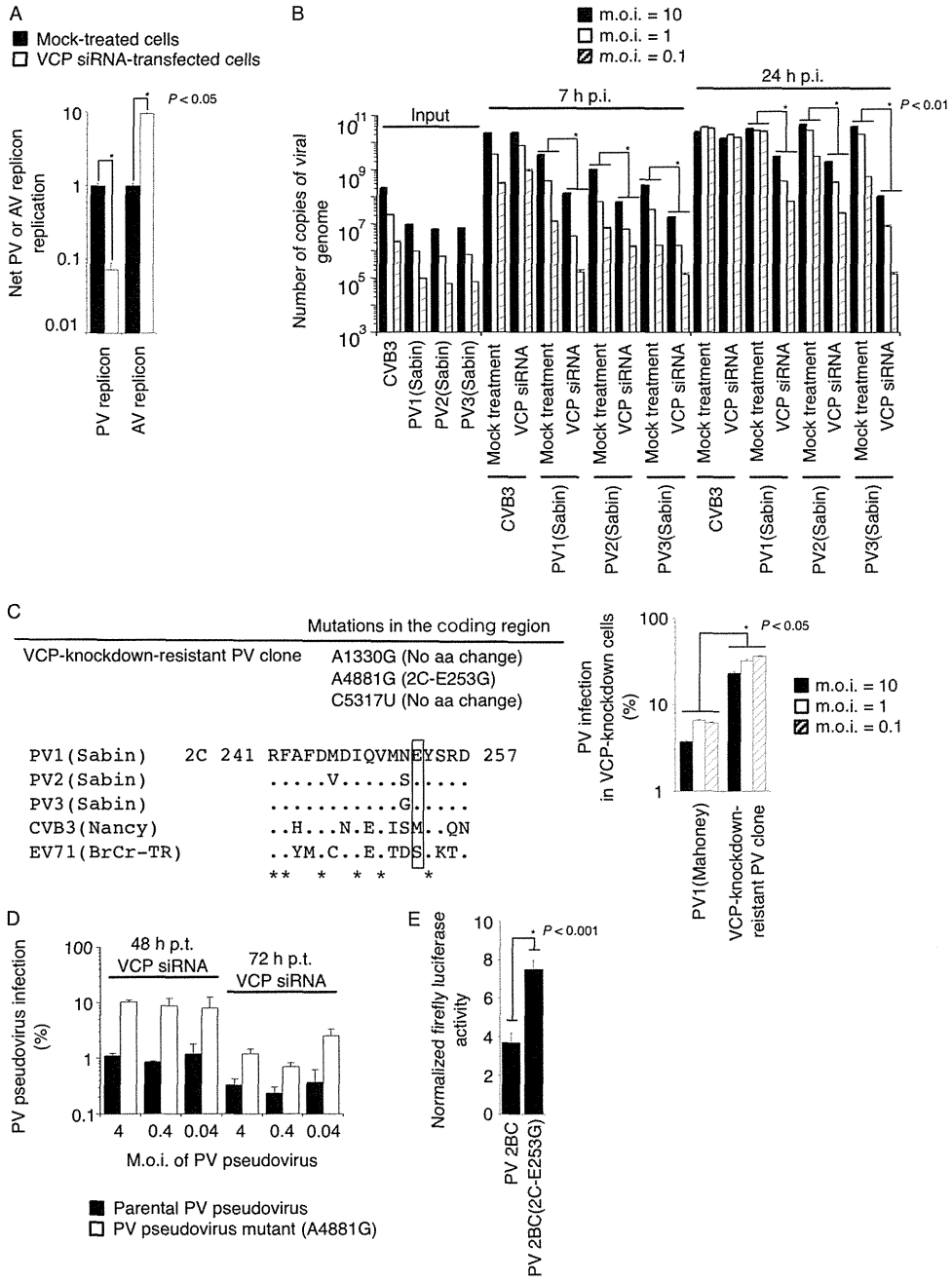

FIG 6 VCP act as a PV-specific host factor of viral replication via a cellular secretion pathway. (A) Effect of VCP-siRNA treatment on PV and AV replicon replication. Luciferase activity in mock-treated and VCP-siRNA-transfected cells was analyzed at 7 h p.t. of RNA transcripts of each replicon. (B) Effect of VCP-siRNA treatment on CVB3 and type 1, 2, and 3 PV infection. Cells were infected with CVB3 or type 1, 2, and 3 PV (Sabin) at an MOI of 10, 1, or 0.1, and then the amounts of viral genome in the infected cells were analyzed at 7 or 24 h p.i. Numbers of copies of the viral genome of input virus and in infected cells are shown. The number of copies of the viral genome in VCP-siRNA-treated cells was compared with that in mock-treated cells infected with viruses at each MOI. (C) Isolation of PV mutant resistant to VCP knockdown. The left panel shows mutations in the coding region of a VCP-knockdown-resistant PV clone (top) and partial 2C sequences around aa 253 (aa 241 to 257 of 2C) of enteroviruses (bottom) are shown. Amino acid 253 is highlighted in a rectangle. Results of a PV infection assay in VCP-knockdown cells are shown at right. VCP-siRNA-transfected or mock-treated HEK293 cells were infected with PV1 (Mahoney) or a VCP-knockdown-resistant PV clone at 48 h p.t. of VCP siRNA at an MOI of 10, 1, and 0.1. Numbers of copies of viral RNA were determined at 7 h p.i. PV infection in VCP-knockdown cells is presented as a percentage of the number of copies of viral RNA in VCP-siRNA-transfected cells compared to that in mock-treated cells (100%). A *t* test was performed between samples for each MOI. (D) Effect of VCP-siRNA treatment on PV pseudovirus infection with an A4881G mutation. VCP-siRNA-transfected HEK293 cells were infected with a parental PV pseudovirus or a PV pseudovirus mutant with an A4881G mutation at an MOI of 4, 0.4, or 0.04 at 48 or 72 h p.t. of VCP-siRNA. Percent PV pseudovirus infection is shown. (E) Mammalian two-hybrid assay for VCP (pBIND-VCP) and PV proteins [pACT-PV 2BC or PV 2BC(2C-E253G)]. Normalized firefly luciferase activities are shown.

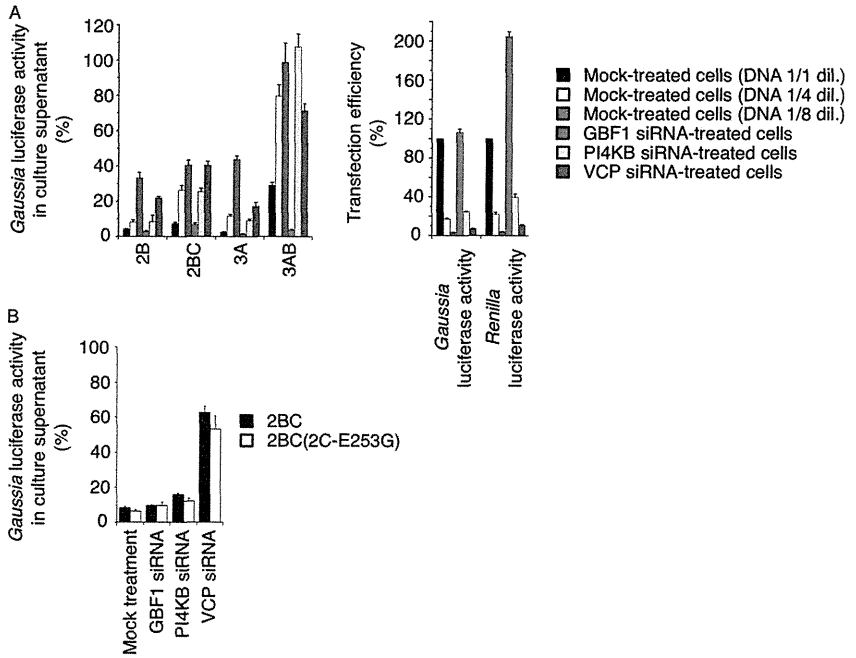

FIG 7 Effect of knockdown of VCP on the inhibition of cellular protein secretion caused by overexpression of each individual viral protein. (A) Inhibition of cellular protein secretion caused by the individual viral protein in siRNA-treated cells. Secretion of *Gaussia* luciferase was analyzed in mock-treated and GBF1-, PI4KB-, and VCP-siRNA-transfected HEK293 cells expressing viral proteins 2B, 2BC, 3A, and 3AB (left). For mock-treated cells, DNAs (control vector and *Gaussia* luciferase expression vector) diluted by 1-, 4-, and 8-fold were transfected to control the transfection efficiency. *Gaussia* luciferase activity in cells transfected with a control expression vector was taken as 100%. At right is an evaluation of DNA transfection efficiency. *Gaussia* luciferase activity in the cells transfected with a control vector and *Gaussia* luciferase expression vector and *Renilla* luciferase activity in the cells transfected with *Renilla* luciferase expression vector are shown as percentages. (B) Effect of a 2C-E253G mutation on the inhibition of cellular protein secretion caused by overexpression of 2BC protein in siRNA-treated cells. *Gaussia* luciferase activity was determined in siRNA-transfected cells, with the value for cells transfected with a control expression vector taken as 100%.

binding proteins that share colocalization with viral proteins. In cells transiently overexpressing viral proteins, 2BC and 3AB showed clear colocalization with VCP (Fig. 4A), consistent with the observations in PV-infected cells. Although VCP has a role in autophagosome formation, the localization of VCP in PV-infected cells seems different from that of the autophagosome marker protein LC3, which showed clear colocalization with 3A in PV-infected cells (48). We observed colocalization of 3A with dsRNA and PI4KB, but not with VCP, in PV-infected cells (Fig. 2 and 3). This suggested that VCP might not be directly involved in autophagosome formation in PV replication or have only a temporal role in autophagosome formation. VCP interacted with the C-terminal region of 3AB (aa 42 to 87 of 3A) in contrast to GBF1 and PI4KB, which interacted with 3AB via the N-terminal region of 3A (aa 1 to 41 of 3A) (Fig. 4B) (33, 43, 86, 91). This suggested that the interaction of VCP with 3AB occurs independently of that of GBF1/PI4KB. Interestingly, the effect of VCP knockdown on viral replication is different among the picornaviruses, with strong suppression for PV, apparently no effect for CVB3, and enhancement for AV (Fig. 6A and B). This observation might suggest some alternative/opposite pathways used for replication of these viruses or a difference in the expression levels of VCP required for optimal replication of these viruses. Interestingly, a VCP orthologue has been identified as a host factor required for the infection of *Drosophila* C virus, which belongs to *Dicistroviridae*, in an siRNA screening (22). This might provide a marked contrast to the broad spectrum of GBF1 and PI4KB as host factors in picornaviruses. GBF1 also could act as a host factor for HCV, a member of the *Flaviviridae* (36), and PI4KA might play the corresponding role of PI4KB in HCV replication for recruitment of viral polymerase (14, 43). These observations suggested that VCP and GBF1/PI4KB have different roles in PV replication via their interactions with 2BC/3AB and 3A/3AB, respectively.

To further analyze the function of VCP in PV replication, we isolated a PV mutant resistant to VCP knockdown (Fig. 6C). The isolated mutant had the mutation A4881G (2C-E253G), which is known as a determinant of a secretion inhibition-negative phenotype of PV (19), as the determinant of the resistance phenotype. The resistance phenotype of this PV mutant was weaker in cells treated by VCP-siRNA for 72 h than that observed in cells treated for 48 h (Fig. 6D), suggesting that VCP is required even for the replication of this VCP-knockdown-resistant PV mutant. Consistent with this observation, increased affinity between 2BC and VCP was observed with a 2C-E253G mutation (Fig. 6E). This might have an analogy with a BFA-resistant PV mutant, which retained dependency on GBF1 for its replication (13). A PV mutant with a 2C-E253G mutation was originally identified by selecting PV-infected cells that expressed newly synthesized surface proteins by using cell sorting (19). However, the origin of the selection pressure or responsible host factors for the emergence of this secretion inhibition-negative mutant remained to be identified. Our results suggested a positive role of VCP in inhibition of cellular protein secretion in PV-infected cells and enhancement of viral RNA replication that might have acted as the selection pressure on the emergence of a secretion inhibition-negative PV mutant. The positive role of VCP in cellular protein secretion was not

detected with an ATPase activity-deficient VCP mutant that did not affect Golgi structure or cellular protein secretion but caused an accumulation of ubiquitinated protein degradation in the ER and ER swelling (28). We could not observe the positive involvement of VCP in the inhibition of cellular protein secretion caused by overexpression of the viral proteins 2B, 2BC, 3A, and 3AB (Fig. 7). To date, overexpression analysis of viral proteins identified 2B/2BC and 3A as the viral proteins responsible for cellular protein secretion (34), and analysis of PV mutants with the secretion-inhibition-negative phenotype identified 2C and 3A as the determinants of the phenotype (15, 19, 32). Our result suggested that VCP acted as a selection pressure on PV for the secretion inhibition-negative phenotype in the infection but was not involved in the inhibition of cellular protein secretion caused by overexpression of individual viral proteins.

VCP colocalizes with ubiquitin-positive inclusions known as aggresomes in various neurodegenerative diseases, including polyglutamine diseases (42, 45, 61), and are involved in aggresome formation and clearance of the aggregate (49, 53, 54, 96). Aggresome formation plays diverse roles in virus infection, including virus factory formation, replication, and packaging of DNA viruses (reviewed in reference 94; 39, 58).The role of VCP in PV replication, possibly via the VCP/3AB/2BC protein complex, remains to be further elucidated.

In summary, we identified VCP as a host factor required for viral RNA replication of PV among membrane-trafficking proteins and found that VCP acted as a selection pressure on PV for the secretion inhibition-negative phenotype. VCP could provide a novel link between the cellular protein secretion pathway and PV replication.

ACKNOWLEDGMENTS

We are grateful to Junko Wada for her excellent technical assistance. We appreciate Akira Kakizuka and Seiji Hori for kindly providing us expression vectors for VCP mutants with helpful suggestions. We appreciate Jun Sasaki for kindly providing us a cDNA clone of AV replicon. We appreciate Takashi Shimoike for kind help in immunofluorescence microscopy.

This study was supported in part by Grants-in-Aid for the Promotion of Polio Eradication and Research on Emerging and Re-emerging Infectious Diseases from the Ministry of Health, Labor and Welfare, Japan, and by a grant from the World Health Organization for a collaborative research project of the Global Polio Eradication Initiative.

REFERENCES

1. **Arita M, Ami Y, Wakita T, Shimizu H.** 2008. Cooperative effect of the attenuation determinants derived from poliovirus Sabin 1 strain is essential for attenuation of enterovirus 71 in the NOD/SCID mouse infection model. J. Virol. **82**:1787–1797.
2. **Arita M, Horie H, Arita M, Nomoto A.** 1999. Interaction of poliovirus with its receptor affords a high level of infectivity to the virion in poliovirus infections mediated by the Fc receptor. J. Virol. **73**:1066–1074.
3. **Arita M, et al.** 2011. Phosphatidylinositol 4-kinase III beta is a target of enviroxime-like compounds for antipoliovirus activity. J. Virol. **85**:2364–2372.
4. **Arita M, Nagata N, Sata T, Miyamura T, Shimizu H.** 2006. Quantitative analysis of poliomyelitis-like paralysis in mice induced by a poliovirus replicon. J. Gen. Virol. **87**:3317–3327.
5. **Arita M, Takebe Y, Wakita T, Shimizu H.** 2010. A bifunctional anti-enterovirus compound that inhibits replication and early stage of enterovirus 71 infection. J. Gen. Virol. **91**:2734–2744.
6. **Arita M, Wakita T, Shimizu H.** 2009. Cellular kinase inhibitors that suppress enterovirus replication have a conserved target in viral protein 3A similar to that of enviroxime. J. Gen. Virol. **90**:1869–1879.
7. **Arita M, Wakita T, Shimizu H.** 2008. Characterization of pharmacologically active compounds that inhibit poliovirus and enterovirus 71 infectivity. J. Gen. Virol. **89**:2518–2530.
8. **Arita M, et al.** 2005. A Sabin 3-derived poliovirus recombinant contained a sequence homologous with indigenous human enterovirus species C in the viral polymerase coding region. J. Virol. **79**:12650–12657.
9. **Barnard DL.** 2006. Current status of anti-picornavirus therapies. Curr. Pharm. Des. **12**:1379–1390.
10. **Barton DJ, Flanegan JB.** 1997. Synchronous replication of poliovirus RNA: initiation of negative-strand RNA synthesis requires the guanidine-inhibited activity of protein 2C. J. Virol. **71**:8482–8489.
11. **Belov GA, Feng Q, Nikovics K, Jackson CL, Ehrenfeld E.** 2008. A critical role of a cellular membrane traffic protein in poliovirus RNA replication. PLoS Pathog. **4**:e1000216.
12. **Belov GA, Habbersett C, Franco D, Ehrenfeld E.** 2007. Activation of cellular Arf GTPases by poliovirus protein 3CD correlates with virus replication. J. Virol. **81**:9259–9267.
13. **Belov GA, Kovtunovych G, Jackson CL, Ehrenfeld E.** 2010. Poliovirus replication requires the N-terminus but not the catalytic Sec7 domain of ArfGEF GBF1. Cell. Microbiol. **12**:1463–1479.
14. **Berger KL, et al.** 2009. Roles for endocytic trafficking and phosphatidylinositol 4-kinase III alpha in hepatitis C virus replication. Proc. Natl. Acad. Sci. U. S. A. **106**:7577–7582.
15. **Berstein HD, Baltimore D.** 1988. Poliovirus mutant that contains a cold-sensitive defect in viral RNA synthesis. J. Virol. **62**:2922–2928.
16. **Bienz K, Egger D, Troxler M, Pasamontes L.** 1990. Structural organization of poliovirus RNA replication is mediated by viral proteins of the P2 genomic region. J. Virol. **64**:1156–1163.
17. **Bodian D.** 1949. Histopathologic basis of clinical findings in poliomyelitis. Am. J. Med. **6**:563–578.
18. **Brown-Augsburger P, et al.** 1999. Evidence that enviroxime targets multiple components of the rhinovirus 14 replication complex. Arch. Virol. **144**:1569–1585.
19. **Burgon TB, Jenkins JA, Deitz SB, Spagnolo JF, Kirkegaard K.** 2009. Bypass suppression of small-plaque phenotypes by a mutation in poliovirus 2A that enhances apoptosis. J. Virol. **83**:10129–10139.
20. **Caliguiri LA, Tamm I.** 1968. Action of guanidine on the replication of poliovirus RNA. Virology **35**:408–417.
21. **Chen TC, et al.** 2008. Development of antiviral agents for enteroviruses. J. Antimicrob. Chemother. **62**:1169–1173.
22. **Cherry S, et al.** 2006. COPI activity coupled with fatty acid biosynthesis is required for viral replication. PLoS Pathog. **2**:e102.
23. **Choe SS, Dodd DA, Kirkegaard K.** 2005. Inhibition of cellular protein secretion by picornaviral 3A proteins. Virology **337**:18–29.
24. **Collett MS, Neyts J, Modlin JF.** 2008. A case for developing antiviral drugs against polio. Antiviral Res. **79**:179–187.
25. **Committee on Development of a Polio Antiviral and Its Potential Role in Global Poliomyelitis Eradication, National Research Council.** 2006. Exploring the role of antiviral drugs in the eradication of polio: workshop report. National Academies Press, Washington, DC.
26. **Couderc T, et al.** 1989. Molecular pathogenesis of neural lesions induced by poliovirus type 1. J. Gen. Virol. **70**:2907–2918.
27. **Cuconati A, Molla A, Wimmer E.** 1998. Brefeldin A inhibits cell-free, de novo synthesis of poliovirus. J. Virol. **72**:6456–6464.
28. **Dalal S, Rosser MF, Cyr DM, Hanson PI.** 2004. Distinct roles for the AAA ATPases NSF and p97 in the secretory pathway. Mol. Biol. Cell **15**: 637–648.
29. **Datta U, Dasgupta A.** 1994. Expression and subcellular localization of poliovirus VPg-precursor protein 3AB in eukaryotic cells: evidence for glycosylation in vitro. J. Virol. **68**:4468–4477.
30. **De Palma AM, et al.** 2008. The thiazolobenzimidazole TBZE-029 inhibits enterovirus replication by targeting a short region immediately downstream from motif C in the nonstructural protein 2C. J. Virol. **82**:4720–4730.
31. **De Palma AM, et al.** 2009. Mutations in the nonstructural protein 3A confer resistance to the novel enterovirus replication inhibitor TTP-8307. Antimicrob. Agents Chemother. **53**:1850–1857.
32. **Dodd DA, Giddings TH, Jr, Kirkegaard K.** 2001. Poliovirus 3A protein limits interleukin-6 (IL-6), IL-8, and beta interferon secretion during viral infection. J. Virol. **75**:8158–8165.
33. **Doedens Jr, Giddings TH, Jr, Kirkegaard K.** 1997. Inhibition of endoplasmic reticulum-to-Golgi traffic by poliovirus protein 3A: genetic and ultrastructural analysis. J. Virol. **71**:9054–9064.

34. **Doedens JR, Kirkegaard K.** 1995. Inhibition of cellular protein secretion by poliovirus proteins 2B and 3A. EMBO J. **14**:894–907.
35. **Eggers HJ, Tamm I.** 1961. Spectrum and characteristics of the virus inhibitory action of 2-(alpha-hydroxybenzyl)-benzimidazole. J. Exp. Med. **113**:657–682.
36. **Goueslain L, et al.** 2010. Identification of GBF1 as a cellular factor required for hepatitis C virus RNA replication. J. Virol. **84**:773–787.
37. **Greninger AL, Knudsen GM, Betegon M, Burlingame AL, Derisi JL.** 18 January 2012. The 3A protein from multiple picornaviruses utilizes the Golgi adaptor protein ACBD3 to recruit PI4KIIIβ. J. Virol. **86**:3605–3616.
38. **Halawani D, et al.** 2009. Hereditary inclusion body myopathy-linked p97/VCP mutations in the NH2 domain and the D1 ring modulate p97/VCP ATPase activity and D2 ring conformation. Mol. Cell. Biol. **29**:4484–4494.
39. **Heath CM, Windsor M, Wileman T.** 2001. Aggresomes resemble sites specialized for virus assembly. J. Cell Biol. **153**:449–455.
40. **Heinz BA, Vance LM.** 1995. The antiviral compound enviroxime targets the 3A coding region of rhinovirus and poliovirus. J. Virol. **69**:4189–4197.
41. **Hetzer M, et al.** 2001. Distinct AAA-ATPase p97 complexes function in discrete steps of nuclear assembly. Nat. Cell Biol. **3**:1086–1091.
42. **Hirabayashi M, et al.** 2001. VCP/p97 in abnormal protein aggregates, cytoplasmic vacuoles, and cell death, phenotypes relevant to neurodegeneration. Cell Death Differ. **8**:977–984.
43. **Hsu NY, et al.** 2010. Viral reorganization of the secretory pathway generates distinct organelles for RNA replication. Cell **141**:799–811.
44. **Irurzun A, Perez L, Carrasco L.** 1992. Involvement of membrane traffic in the replication of poliovirus genomes: effects of brefeldin A. Virology **191**:166–175.
45. **Ishigaki S, et al.** 2004. Physical and functional interaction between Dorfin and Valosin-containing protein that are colocalized in ubiquitylated inclusions in neurodegenerative disorders. J. Biol. Chem. **279**:51376–51385.
46. **Ishikawa K, Sasaki J, Taniguchi K.** 2010. Overall linkage map of the nonstructural proteins of Aichi virus. Virus Res. **147**:77–84.
47. **Ishitsuka H, Ohsawa C, Ohiwa T, Umeda I, Suhara Y.** 1982. Antipicornavirus flavone Ro 09-0179. Antimicrob. Agents Chemother. **22**:611–616.
48. **Jackson WT, et al.** 2005. Subversion of cellular autophagosomal machinery by RNA viruses. PLoS Biol. **3**:e156.
49. **Johnston JA, Ward CL, Kopito RR.** 1998. Aggresomes: a cellular response to misfolded proteins. J. Cell Biol. **143**:1883–1898.
50. **Ju JS, et al.** 2009. Valosin-containing protein (VCP) is required for autophagy and is disrupted in VCP disease. J. Cell Biol. **187**:875–888.
51. **Ju JS, Miller SE, Hanson PI, Weihl CC.** 2008. Impaired protein aggregate handling and clearance underlie the pathogenesis of p97/VCP-associated disease. J. Biol. Chem. **283**:30289–30299.
52. **Ju JS, Weihl CC.** 2010. p97/VCP at the intersection of the autophagy and the ubiquitin proteasome system. Autophagy **6**:283–285.
53. **Kitami MI, et al.** 2006. Dominant-negative effect of mutant valosin-containing protein in aggresome formation. FEBS Lett. **580**:474–478.
54. **Kobayashi T, Manno A, Kakizuka A.** 2007. Involvement of valosin-containing protein (VCP)/p97 in the formation and clearance of abnormal protein aggregates. Genes Cells **12**:889–901.
55. **Kobayashi T, Tanaka K, Inoue K, Kakizuka A.** 2002. Functional ATPase activity of p97/valosin-containing protein (VCP) is required for the quality control of endoplasmic reticulum in neuronally differentiated mammalian PC12 cells. J. Biol. Chem. **277**:47358–47365.
56. **Koller KJ, Brownstein MJ.** 1987. Use of a cDNA clone to identify a supposed precursor protein containing valosin. Nature **325**:542–545.
57. **Laemmli UK.** 1970. Cleavage of structural proteins during the assembly of the head of bacteriophage T4. Nature **227**:680–685.
58. **Liu Y, Shevchenko A, Berk AJ.** 2005. Adenovirus exploits the cellular aggresome response to accelerate inactivation of the MRN complex. J. Virol. **79**:14004–14016.
59. **Manno A, Noguchi M, Fukushi J, Motohashi Y, Kakizuka A.** 2010. Enhanced ATPase activities as a primary defect of mutant valosin-containing proteins that cause inclusion body myopathy associated with Paget disease of bone and frontotemporal dementia. Genes Cells **15**:911–922.
60. **Maynell LA, Kirkegaard K, Klymkowsky MW.** 1992. Inhibition of poliovirus RNA synthesis by brefeldin A. J. Virol. **66**:1985–1994.
61. **Mizuno Y, Hori S, Kakizuka A, Okamoto K.** 2003. Vacuole-creating protein in neurodegenerative diseases in humans. Neurosci. Lett. **343**:77–80.
62. **Moffat K, et al.** 2005. Effects of foot-and-mouth disease virus nonstructural proteins on the structure and function of the early secretory pathway: 2BC but not 3A blocks endoplasmic reticulum-to-Golgi transport. J. Virol. **79**:4382–4395.
63. **Nagashima S, Sasaki J, Taniguchi K.** 2003. Functional analysis of the stem-loop structures at the 5′ end of the Aichi virus genome. Virology **313**:56–65.
64. **Nowis D, McConnell E, Wojcik C.** 2006. Destabilization of the VCP-Ufd1-Npl4 complex is associated with decreased levels of ERAD substrates. Exp. Cell Res. **312**:2921–2932.
65. **Peters JM, Walsh MJ, Franke WW.** 1990. An abundant and ubiquitous homo-oligomeric ring-shaped ATPase particle related to the putative vesicle fusion proteins Sec18p and NSF. EMBO J. **9**:1757–1767.
66. **Peyroche A, et al.** 1999. Brefeldin A acts to stabilize an abortive ARF-GDP-Sec7 domain protein complex: involvement of specific residues of the Sec7 domain. Mol. Cell **3**:275–285.
67. **Pierini R, Cottam E, Roberts R, Wileman T.** 2009. Modulation of membrane traffic between endoplasmic reticulum, ERGIC and Golgi to generate compartments for the replication of bacteria and viruses. Semin. Cell Dev. Biol. **20**:828–833.
68. **Rabouille C, Levine TP, Peters JM, Warren G.** 1995. An NSF-like ATPase, p97, and NSF mediate cisternal regrowth from mitotic Golgi fragments. Cell **82**:905–914.
69. **Ramadan K, et al.** 2007. Cdc48/p97 promotes reformation of the nucleus by extracting the kinase Aurora B from chromatin. Nature **450**:1258–1262.
70. **Rotbart HA.** 2002. Treatment of picornavirus infections. Antiviral Res. **53**:83–98.
71. **Roy L, et al.** 2000. Role of p97 and syntaxin 5 in the assembly of transitional endoplasmic reticulum. Mol. Biol. Cell **11**:2529–2542.
72. **Sabin AB.** 1965. Oral poliovirus vaccine. History of its development and prospects for eradication of poliomyelitis. JAMA **194**:872–876.
73. **Salk JE, et al.** 1954. Studies in human subjects on active immunization against poliomyelitis. II. A practical means for inducing and maintaining antibody formation. Am. J. Public Health Nations Health **44**:994–1009.
74. **Sandoval IV, Carrasco L.** 1997. Poliovirus infection and expression of the poliovirus protein 2B provoke the disassembly of the Golgi complex, the organelle target for the antipoliovirus drug Ro-090179. J. Virol. **71**:4679–4693.
75. **Sasaki J, Ishikawa K, Arita M, Taniguchi K.** 2012. ACBD3-mediated recruitment of PI4KB to picornavirus RNA replication sites. EMBO J. **31**:754–766.
76. **Schroder R, et al.** 2005. Mutant valosin-containing protein causes a novel type of frontotemporal dementia. Ann. Neurol. **57**:457–461.
77. **Shimizu H, et al.** 2000. Mutations in the 2C region of poliovirus responsible for altered sensitivity to benzimidazole derivatives. J. Virol. **74**:4146–4154.
78. **Sledz CA, Holko M, de Veer MJ, Silverman RH, Williams BR.** 2003. Activation of the interferon system by short-interfering RNAs. Nat. Cell Biol. **5**:834–839.
79. **Soderberg O, et al.** 2006. Direct observation of individual endogenous protein complexes in situ by proximity ligation. Nat. Methods **3**:995–1000.
80. **Sohda M, et al.** 2001. Identification and characterization of a novel Golgi protein, GCP60, that interacts with the integral membrane protein giantin. J. Biol. Chem. **276**:45298–45306.
81. **Strauss DM, Glustrom LW, Wuttke DS.** 2003. Towards an understanding of the poliovirus replication complex: the solution structure of the soluble domain of the poliovirus 3A protein. J. Mol. Biol. **330**:225–234.
82. **Suhy DA, Giddings TH, Jr, Kirkegaard K.** 2000. Remodeling the endoplasmic reticulum by poliovirus infection and by individual viral proteins: an autophagy-like origin for virus-induced vesicles. J. Virol. **74**:8953–8965.
83. **Tang WF, et al.** 2007. Reticulon 3 binds the 2C protein of enterovirus 71 and is required for viral replication. J. Biol. Chem. **282**:5888–5898.
84. **Taylor MP, Burgon TB, Kirkegaard K, Jackson WT.** 2009. Role of microtubules in extracellular release of poliovirus. J. Virol. **83**:6599–6609.
85. **Teterina NL, et al.** 2006. Evidence for functional protein interactions required for poliovirus RNA replication. J. Virol. **80**:5327–5337.
86. **Teterina NL, Pinto Y, Weaver JD, Jensen KS, Ehrenfeld E.** 2011. Analysis of poliovirus protein 3A interactions with viral and cellular proteins in infected cells. J. Virol. **85**:4284–4296.
87. **Tresse E, et al.** 2010. VCP/p97 is essential for maturation of ubiquitin-

containing autophagosomes and this function is impaired by mutations that cause IBMPFD. Autophagy 6:217–227.
88. **Watts GD, et al.** 2004. Inclusion body myopathy associated with Paget disease of bone and frontotemporal dementia is caused by mutant valosin-containing protein. Nat. Genet. 36:377–381.
89. **Weihl CC, Dalal S, Pestronk A, Hanson PI.** 2006. Inclusion body myopathy-associated mutations in p97/VCP impair endoplasmic reticulum-associated degradation. Hum. Mol. Genet. 15:189–199.
90. **Weihl CC, Miller SE, Hanson PI, Pestronk A.** 2007. Transgenic expression of inclusion body myopathy associated mutant p97/VCP causes weakness and ubiquitinated protein inclusions in mice. Hum. Mol. Genet. 16:919–928.
91. **Wessels E, et al.** 2006. A viral protein that blocks Arf1-mediated COP-I assembly by inhibiting the guanine nucleotide exchange factor GBF1. Dev. Cell 11:191–201.
92. **White SR, Lauring B.** 2007. AAA+ ATPases: achieving diversity of function with conserved machinery. Traffic 8:1657–1667.
93. **Wikel JH, et al.** 1980. Synthesis of syn and anti isomers of 6-[[(hydroxyimino)phenyl]methyl]-1-[(1-methylethyl)sulfonyl]-1H-benzimidaz ol-2-amine. Inhibitors of rhinovirus multiplication. J. Med. Chem. 23:368–372.
94. **Wileman T.** 2006. Aggresomes and autophagy generate sites for virus replication. Science 312:875–878.
95. **Wojcik C, et al.** 2006. Valosin-containing protein (p97) is a regulator of endoplasmic reticulum stress and of the degradation of N-end rule and ubiquitin-fusion degradation pathway substrates in mammalian cells. Mol. Biol. Cell 17:4606–4618.
96. **Wojcik C, Yano M, DeMartino GN.** 2004. RNA interference of valosin-containing protein (VCP/p97) reveals multiple cellular roles linked to ubiquitin/proteasome-dependent proteolysis. J. Cell Sci. 117: 281–292.
97. **Yamashita T, et al.** 1998. Complete nucleotide sequence and genetic organization of Aichi virus, a distinct member of the *Picornaviridae* associated with acute gastroenteritis in humans. J. Virol. 72:8408–8412.

JVI
Journals.ASM.org

The Toll-Like Receptor 3-Mediated Antiviral Response Is Important for Protection against Poliovirus Infection in Poliovirus Receptor Transgenic Mice

Yuko Abe,[a] Ken Fujii,[a] Noriyo Nagata,[b] Osamu Takeuchi,[c] Shizuo Akira,[c] Hiroyuki Oshiumi,[d] Misako Matsumoto,[d] Tsukasa Seya,[d] and Satoshi Koike[a]

Neurovirology Project, Tokyo Metropolitan Institute of Medical Science, 2-1-6 Kamikitazawa, Setagaya-ku, Tokyo 156-8506, Japan[a]; Department of Pathology, National Institute of Infectious Diseases, 4-7-1 Gakuen, Musashimurayama, Tokyo 208-0011, Japan[b]; Laboratory of Host Defense, WPI Immunology Frontier Research Center (IFReC), Osaka University, 3-1 Yamada-oka, Suita, Osaka 565-0871, Japan[c]; and Department of Microbiology and Immunology, Hokkaido University Graduate School of Medicine, Kita 15, Nishi 7, Kita-ku, Sapporo 060-8638, Japan[d]

RIG-I-like receptors and Toll-like receptors (TLRs) play important roles in the recognition of viral infections. However, how these molecules contribute to the defense against poliovirus (PV) infection remains unclear. We characterized the roles of these sensors in PV infection in transgenic mice expressing the PV receptor. We observed that alpha/beta interferon (IFN-α/β) production in response to PV infection occurred in an MDA5-dependent but RIG-I-independent manner in primary cultured kidney cells *in vitro*. These results suggest that, similar to the RNA of other picornaviruses, PV RNA is recognized by MDA5. However, serum IFN-α levels, the viral load in nonneural tissues, and mortality rates did not differ significantly between MDA5-deficient mice and wild-type mice. In contrast, we observed that serum IFN production was abrogated and that the viral load in nonneural tissues and mortality rates were both markedly higher in TIR domain-containing adaptor-inducing IFN-β (TRIF)-deficient and TLR3-deficient mice than in wild-type mice. The mortality rate of MyD88-deficient mice was slightly higher than that of wild-type mice. These results suggest that multiple pathways are involved in the antiviral response in mice and that the TLR3-TRIF-mediated signaling pathway plays an essential role in the antiviral response against PV infection.

Poliovirus (PV), which belongs to the genus *Enterovirus* in the family *Picornaviridae*, is the causative agent of poliomyelitis (38). The host range of PV is restricted to primates (18). This species' tropism is determined primarily by the cellular PV receptor (PVR; CD155), which gives the virus access to susceptible cells (14–16, 20). Mice are generally not susceptible to PV. However, transgenic mice expressing human PVR (PVR-tg mice) become susceptible to PV and develop a paralytic disease similar to human poliomyelitis after the administration of PV intravenously, intraperitoneally, intracerebrally, or intramuscularly but not orally (26, 40). PV shows a neurotropic phenotype in both humans and PVR-tg mice. PV preferentially replicates in neurons, especially in motor neurons in the anterior or ventral horn of the spinal cord and in the brainstem. However, the efficiency of PV replication is low in nonneural tissues (4, 25). We previously found that innate immune responses that are mediated by type I interferons (IFNs) play important roles in controlling viral replication in nonneural tissues and in the mortality rates of PVR-tg mice (19). In PVR-tg mice deficient in IFNAR1, PV efficiently replicates in nonneural tissues such as the liver, pancreas, and spleen, which are not normal targets of PV. IFNAR1-deficient mice die after the inoculation of a small amount of PV by peripheral routes. The results suggest that the type I IFN response forms an innate immune barrier that prevents PV replication in nonneural tissues and subsequent PV invasion of the central nervous system (CNS). This response therefore plays important roles in the tissue tropism and pathogenicity of PV (25).

The sensors that are involved in the production of type I IFNs in response to RNA viral infections have been recently identified and characterized (1, 46–48). The RIG-I-like receptors (RLRs) retinoic-acid-inducible gene 1 (RIG-I) and melanoma differentiation-associated gene 5 (MDA5) are expressed in the cytoplasm of all cell types, with the exception of plasmacytoid dendritic cells (pDCs). RIG-I and MDA5 have RNA binding domains and differentially recognize specific characteristics of nonself viral RNAs (17, 22, 36, 37). In addition, RLRs have DExD/H box RNA helicase domains (51) that activate downstream signaling pathways resulting in the activation of IFN regulatory factor 3 (IRF-3) and IRF-7 (53). TLR3 and TLR7 are the sensors for viral double-stranded RNA (dsRNA) and single-stranded RNA, respectively (2, 8, 12). TLR3 is expressed in the endosome of macrophages and conventional dendritic cells (DCs) (28) but not in pDCs. TLR3 is also expressed in a variety of epithelial cells, including airway, uterine, corneal, vaginal, cervical, biliary, and intestinal epithelial cells, which may function as efficient barriers to infection. The TLR3-mediated signaling pathway is transmitted through Toll–interleukin-1 (IL-1) receptor (TIR)-containing adaptor molecule 1, which is also known as TIR domain-containing adaptor inducing IFN-β (TRIF), and finally results in the activation of IRF3 and IRF7 (13, 34, 51). TLR7 is specifically expressed in the endosome of pDCs and contributes to the production of a large amount of IFNs in response to many RNA virus infections (5, 7). TLR7 signaling is mediated by the adaptor molecule myeloid differentiation factor 88 (MyD88). These sensors do not contribute equally

Received 29 May 2011 **Accepted** 20 October 2011
Published ahead of print 9 November 2011
Address correspondence to Satoshi Koike, koike-st@igakuken.or.jp.

doi:10.1128/JVI.05245-11

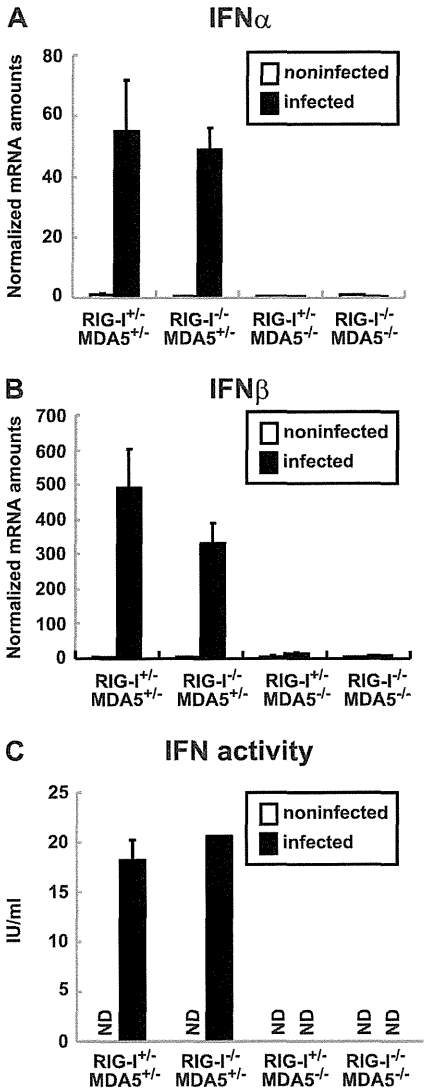

FIG 1 Production of IFNs in primary cultured kidney cells prepared from RIG-I- and MDA5-deficient mice. Kidney cells were pretreated with 100 U of IFN-β for 2 h and infected with PV at an MOI of 10. RNA was prepared from the infected cells at 6 hpi. The amounts of IFN-α mRNA (A) and IFN-β mRNA (B) were determined using quantitative real-time PCR. Cells were prepared in duplicate, and the experiments were repeated three times. Representative data are shown. The amount of IFN activity in the supernatant of infected kidney cells at 8 hpi was determined by the cytopathic effect dye uptake method using L929 cells (C). ND, not detected.

to the antiviral response to each viral infection. The type I IFN production that is induced by these sensors occurs in a virus-specific and cell-specific manner (21, 23). For example, RIG-I plays an important role in the antiviral response to Newcastle disease virus, influenza A virus, Sendai virus, vesicular stomatitis virus, Japanese encephalitis virus, and hepatitis C virus. However, MDA5 is important in the response to infection with picornaviruses, such as encephalomyocarditis virus (EMCV) (10, 23). Although RNA viruses produce dsRNA during the replication step, the protective effect of the TLR3-mediated pathway is not clear (9). In a previous study, TLR3 expression was found to cause severe encephalitis in West Nile virus (WNV) infection (50). How these sensor molecules contribute to the recognition of PV infection is not understood. The aim of the present study was to determine the role of these sensors in the response to PV infection in transgenic mice expressing human PVR. We generated PVR-tg mice deficient in these sensor and adaptor molecules. Our results demonstrate that the MDA5-, TRIF- and MyD88-mediated pathways contribute to the antiviral response against PV infection and that the TLR3-TRIF-mediated pathway plays a pivotal role in this response.

MATERIALS AND METHODS

Cells and viruses. An AGMK cell line, JVK-03 (24), was maintained in Eagle's minimum essential medium containing 5% fetal bovine serum. PV type I Mahoney, a strain derived from the infectious cDNA clone pOM, was used in this study (45). The virus was propagated in JVK-03, and the viral titer was determined using the plaque assay. Primary cultured kidney cells were prepared from transgenic and knockout mice as previously described (54).

Transgenic and knockout mice and infection experiments. All experiments using mice were performed in accordance with the Guidelines for the Care and Use of Laboratory Animals of the Tokyo Metropolitan Institute of Medical Science. ICR-PVRTg21 mice (26) were mated with RIG-I$^{-/-}$ and/or MDA5$^{-/-}$ mice (21) in the ICR background because it is difficult to maintain RIG-I$^{-/-}$ mice in other genetic backgrounds. We mated mice and obtained littermates with the genotypes RIG-I$^{+/-}$ MDA5$^{+/-}$, RIG-I$^{-/-}$ MDA5$^{+/-}$, RIG-I$^{+/-}$ MDA5$^{-/-}$, and RIG-I$^{-/-}$ MDA5$^{-/-}$ to use in experiments. C57BL/6 (B6)-PVRTg21 mice were mated with MDA5$^{-/-}$ mice, TRIF$^{-/-}$ mice, MyD88$^{-/-}$ mice, and TLR3$^{-/-}$ mice (51) in the B6 background (backcrossed 7 to 10 times). IFNAR1$^{-/-}$ PVR-tg mice were previously described (19). Because all of the mice that were used in the present study were in the PVR-tg background, we omitted the notation "PVR-tg" for simplicity in this report. Six- to 7-week-old mice were used for infection experiments. The survival and clinical symptoms of the mice were observed daily for 3 weeks. At the first sign of severe neurological symptoms, the mice were sacrificed as a humane endpoint.

Measurement of IFN levels. IFN-α levels in the sera were determined using an enzyme-linked immunosorbent assay (ELISA). The ELISA kit for IFN-α was purchased from PBL Biochemical Laboratories. Mouse IFN activity in the supernatants of PV-infected kidney cells was measured by the cytopathic effect dye uptake method using L929 cells (54, 55). Recombinant mouse IFN-β (Toray) was used as the standard for unit definition.

Quantitative real-time reverse transcription (RT)-PCR. RNA was isolated from the tissues of infected mice or infected cells using the Isogen RNA extraction kit (Nippon Gene). DNase I treatment and cDNA synthesis were performed as previously described (54). The amounts of the mRNAs for IFN-α, IFN-β, OAS1a, and IRF-7 were determined using real-time RT-PCR with an ABI Prism 7500 (Applied Biosystems) as previously described (54).

RESULTS

IFN production in primary cultured kidney cells is dependent on MDA5. We examined whether, similar to EMCV infection, PV infection is recognized by MDA5 *in vitro*. We mated PVR-tg mice with MDA5-deficient and RIG-I-deficient mice to generate RIG-I$^{+/-}$ MDA5$^{+/-}$, RIG-I$^{-/-}$ MDA5$^{+/-}$, RIG-I$^{+/-}$ MDA5$^{-/-}$, and RIG-I$^{-/-}$ MDA5$^{-/-}$ mice in the ICR background. We prepared primary cultured kidney cells from mice with these genotypes to determine the role of RLRs. After cultivation for approximately 1 week, the cells that became confluent were infected with PV at a multiplicity of infection (MOI) of 10. RNA was recovered from the infected cells at 6 hpi, and the amounts of the mRNAs for IFN-α and IFN-β were determined using real-time RT-PCR. Kid-

ney cells that were not pretreated with IFN-β before PV infection showed rapid cytopathic effect progression and did not produce IFN mRNA (data not shown). This result is consistent with our previous observations (54). We therefore pretreated cells with 100 U of IFN-β for 2 h and infected them with PV. As we reported previously, the IFN-treated kidney cells became resistant to PV infection, PV replication was severely inhibited, and IFN production was observed (54). Under this condition, we determined the sensor responsible for IFN production. We observed the induction of both IFN-α (Fig. 1A) and IFN-β mRNAs (Fig. 1B) in cells that were isolated from RIGI-I$^{+/-}$ MDA5$^{+/-}$ mice and RIGI-I$^{-/-}$ MDA5$^{+/-}$ mice but not from RIGI-I$^{+/-}$ MDA5$^{-/-}$ mice or RIGI-I$^{-/-}$ MDA5$^{-/-}$ mice. The induced IFN proteins were not detected by ELISA due to a very small amount of IFNs produced in the supernatants. However, IFN activity was detected in the supernatants of PV-infected kidney cells prepared from RIGI-I$^{+/-}$ MDA5$^{+/-}$ mice and RIGI-I$^{-/-}$ MDA5$^{+/-}$ mice but not from RIGI-I$^{+/-}$ MDA5$^{-/-}$ mice or RIGI-I$^{-/-}$ MDA5$^{-/-}$ mice using the cytopathic effect dye uptake method (Fig. 1C). These results suggest that PV infection is recognized by MDA5 but not RIG-I in primary murine kidney cells, which is consistent with previous reports demonstrating that MDA5 is essential for the detection of picornaviruses (10, 23). However, MDA5-mediated IFN production was observed only when cells had been primed with a low dose of IFNs.

IFN responses of MDA5-deficient mice are not significantly different from those of wild-type mice. We hypothesized that MDA5 plays an important role in the type I IFN response upon PV infection *in vivo*. We examined the serum IFN-α levels in PVR-tg mice intravenously infected with 2×10^7 PFU of PV using ELISA. Their serum IFN-α level was initially observed at 9 hpi, peaked at 12 hpi, and began to decline at 24 hpi (Fig. 2A). We then determined the serum IFN-α levels of the knockout mice at 12 hpi. Unexpectedly, similar serum IFN-α levels were detected in RIG-I$^{+/-}$ MDA5$^{+/-}$, RIG-I$^{+/-}$ MDA5$^{-/-}$, RIG-I$^{-/-}$ MDA5$^{+/-}$, and RIG$^{-/-}$ MDA5$^{-/-}$ mice infected with PV (Fig. 2B).

We monitored the induction of mRNAs for the IFN-stimulated genes (ISGs), OAS1a (Fig. 3A) and IRF-7 (Fig. 3B), in the brain, spinal cord, liver, spleen, and kidney using real-time RT-PCR. Among the organs tested, the expression levels of these ISGs were the highest in the spleen. However, the expression profiles of these genes were essentially the same in all organs. In accordance with the elevated serum IFN levels, the induction of ISGs in various organs was observed in all mice (Fig. 3A and B). The results suggest that MDA5 does not play a critical role in IFN production and subsequent ISG induction in response to PV infection *in vivo*.

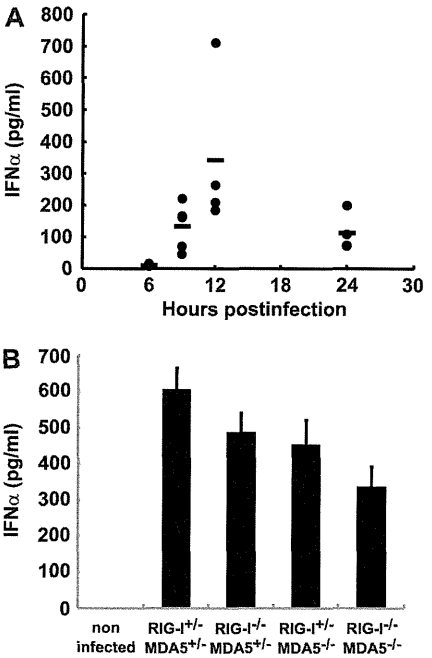

FIG 2 Production of serum IFN-α in RIG-I- and MDA5-deficient mice. (A) Time course of IFN-α levels in serum. PVR-tg mice in the B6 background (n = 4 or n = 5) were intravenously infected with 2×10^7 PFU of PV. Serum samples were collected at the indicated time points, and the concentration of IFN-α was determined using ELISA. (B) IFN-α levels of RIG-I- and MDA5-deficient mice in the ICR background (n = 8) at 12 hpi were compared. The experiments were repeated twice, and representative data are shown.

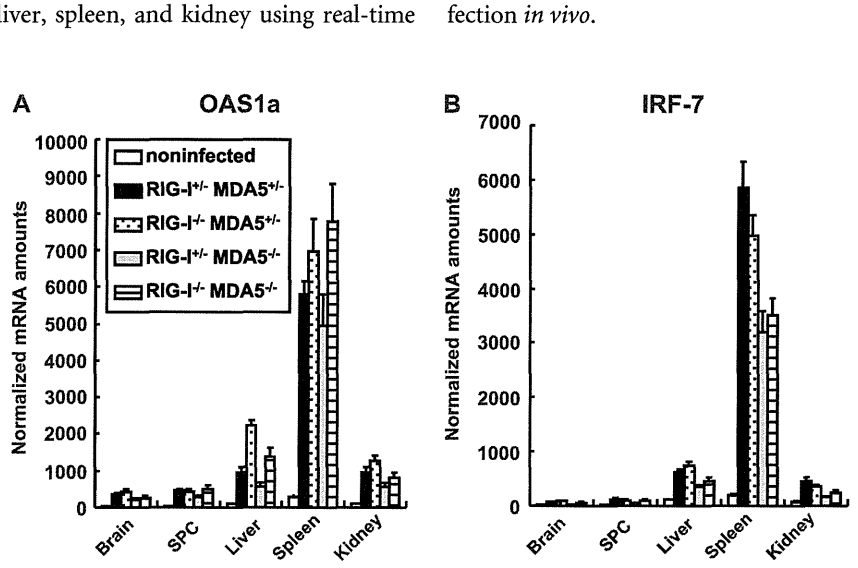

FIG 3 ISG induction in RIG-I- and MDA5-deficient mice. Mice (n = 4) were intravenously infected with 2×10^7 PFU of PV. At 12 hpi, RNA was isolated from the indicated tissues of the infected mice and OAS1a (A) and IRF-7 (B) mRNA levels were determined using quantitative real-time PCR. The experiments were repeated twice, and representative data are shown. SPC, spinal cord.

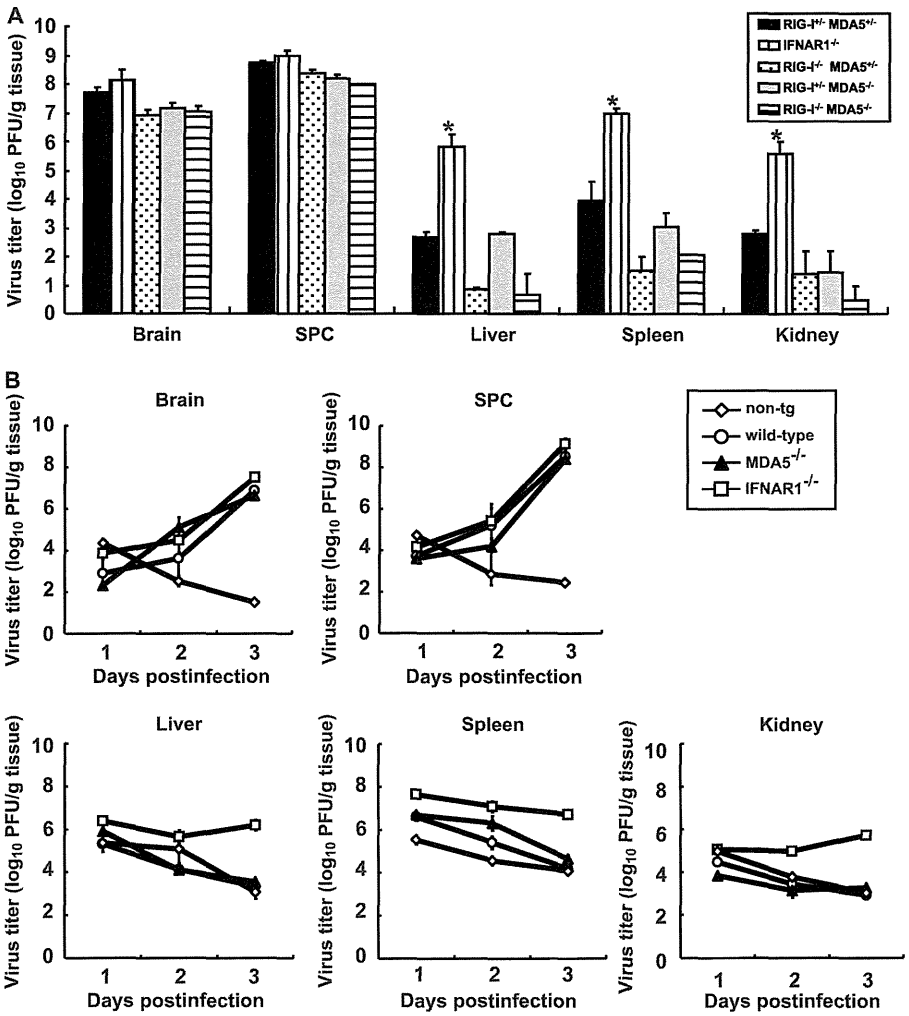

FIG 4 (A) PV replication in RIG-I- and MDA5-deficient mice. RIGI-I$^{+/-}$ MDA5$^{+/-}$, RIGI-I$^{-/-}$ MDA5$^{+/-}$, RIGI-I$^{-/-}$ MDA5$^{+/-}$, and RIGI-I$^{-/-}$ MDA5$^{-/-}$ mice in the ICR background and IFNAR1$^{-/-}$ mice in the B6 background ($n = 3$) were intravenously infected with 2×10^7 PFU of PV. Infected mice were paralyzed or dead at 3 to 5 days postinfection. The tissues of the paralyzed mice were collected, and the viral titers were determined using a plaque assay (*, $P < 0.01$ by t test compared to RIGI-I$^{+/-}$ MDA5$^{+/-}$ mice). (B) PV replication kinetics in MDA5-deficient mice. Nontransgenic (non-tg) mice, wild-type mice, MDA5$^{-/-}$ mice, and IFNAR1$^{-/-}$ mice in the B6 background ($n = 3$) were infected as described above. Tissues were collected daily, and viral titers were determined. SPC, spinal cord.

PV replication in nonneural tissues and mortality rates of mice deficient in RIG-I-like receptors. We have previously shown that the IFN-α/β response forms an innate immune barrier to prevent PV replication in nonneural tissues and PV invasion of the CNS (19, 25). Therefore, we evaluated PV replication in neural and nonneural tissues in RLR-deficient mice. The mice were infected with 2×10^7 PFU of PV, which is approximately 100 times higher than the 50% lethal doses for all mouse strains. The infected mice showed paralysis by 3 to 5 days postinfection. The brain, spinal cord, liver, spleen, and kidney of the paralyzed mice were recovered, and their viral titers were determined (Fig. 4A). PV was recovered from the CNS of the paralyzed mice almost equally among the genotypes. The viral titers recovered from the liver, spleen, and kidney of IFNAR1$^{-/-}$ mice were significantly higher than those of wild-type mice, as previously described (19). However, PV titers that were recovered from these organs of RIG-I$^{-/-}$ MDA5$^{+/-}$, RIG-I$^{+/-}$ MDA5$^{-/-}$, and RIG-I$^{-/-}$ MDA5$^{-/-}$ mice were as low as or lower than those in the organs of RIG-I$^{+/-}$ MDA5$^{+/-}$ mice. We then examined virus replication kinetics using nontransgenic mice, wild-type mice, IFNAR$^{-/-}$ mice, and MDA5$^{-/-}$ mice in the B6 background (Fig. 4B). The viral load in the CNS increased in a similar fashion among the transgenic mouse strains. However, the viral load kinetics in the liver, spleen, and kidney of wild-type and MDA5$^{-/-}$ mice were similar to those of nontransgenic mice. The values for nontransgenic mice indicate the kinetics of clearance of inoculated virus. The results indicated that PV replication was severely inhibited in the liver, spleen, and kidney of wild-type and MDA5$^{-/-}$ mice. This inhibition correlated well with the induction of serum IFNs in MDA5$^{-/-}$ mice (Fig. 2). The PV antigen was detected in neurons in the CNS but not in other tissues in all knockout mice (Table 1). This result indicates that the lack of RLRs did not alter the tissue tropism of PV. These data suggest that inhibition of PV replication in nonneural tissues is not dependent on RLRs and that MDA5-independent mechanisms are the major contributors in controlling PV replication.

We examined the mortality rates of RIG-I$^{+/-}$ MDA5$^{+/-}$, RIG-I$^{-/-}$ MDA5$^{+/-}$, RIG-I$^{+/-}$ MDA5$^{-/-}$, and RIG-I$^{-/-}$ MDA5$^{-/-}$

TABLE 1 PV antigens in RIG-I- and MDA5-deficient mice

Organ or tissue	No. of PV antigen-positive mice/no. of mice tested			
	RIG-I$^{+/-}$ MDA5$^{+/-}$	RIG-I$^{-/-}$ MDA5$^{+/-}$	RIG-I$^{+/-}$ MDA5$^{-/-}$	RIG-I$^{-/-}$ MDA5$^{-/-}$
Brain	4/4	3/3	4/4	4/4
Spinal cord	4/4	3/3	4/4	4/4
Heart	0/4	0/3	0/4	0/4
Lung	0/4	0/3	0/4	0/4
Liver	0/4	0/3	0/4	0/4
Kidney	0/4	0/3	0/4	0/4
Spleen	0/4	0/3	0/4	0/4
Pancreas	0/4	0/3	0/4	0/4
Intestine	0/4	0/3	0/4	0/4
Adipose tissue	0/4	0/3	0/4	0/4

mice in the ICR background after intravenous infection with PV at 10^3, 10^4, and 10^5 PFU (Fig. 5A, B, and C). The mortality rates of these mice did not differ significantly from each other. We observed that the mortality rates of RIG-I$^{+/-}$ MDA5$^{-/-}$ mice that were inoculated with 10^4 PFU of PV was slightly higher than the mice of other genotypes. However, significant differences were not observed in mice that were inoculated with the other doses. Similar experiments were performed using MDA5$^{-/-}$ and MDA5$^{+/-}$ mice in the B6 background (Fig. 5D, E, and F). We did not observe significant differences between the MDA5$^{-/-}$ and MDA5$^{+/-}$ mice. The mortality rate of MDA5$^{-/-}$ mice was slightly higher than that of MDA5$^{+/-}$ mice that were inoculated with 10^5 PFU of PV. However, the opposite trend was observed when mice

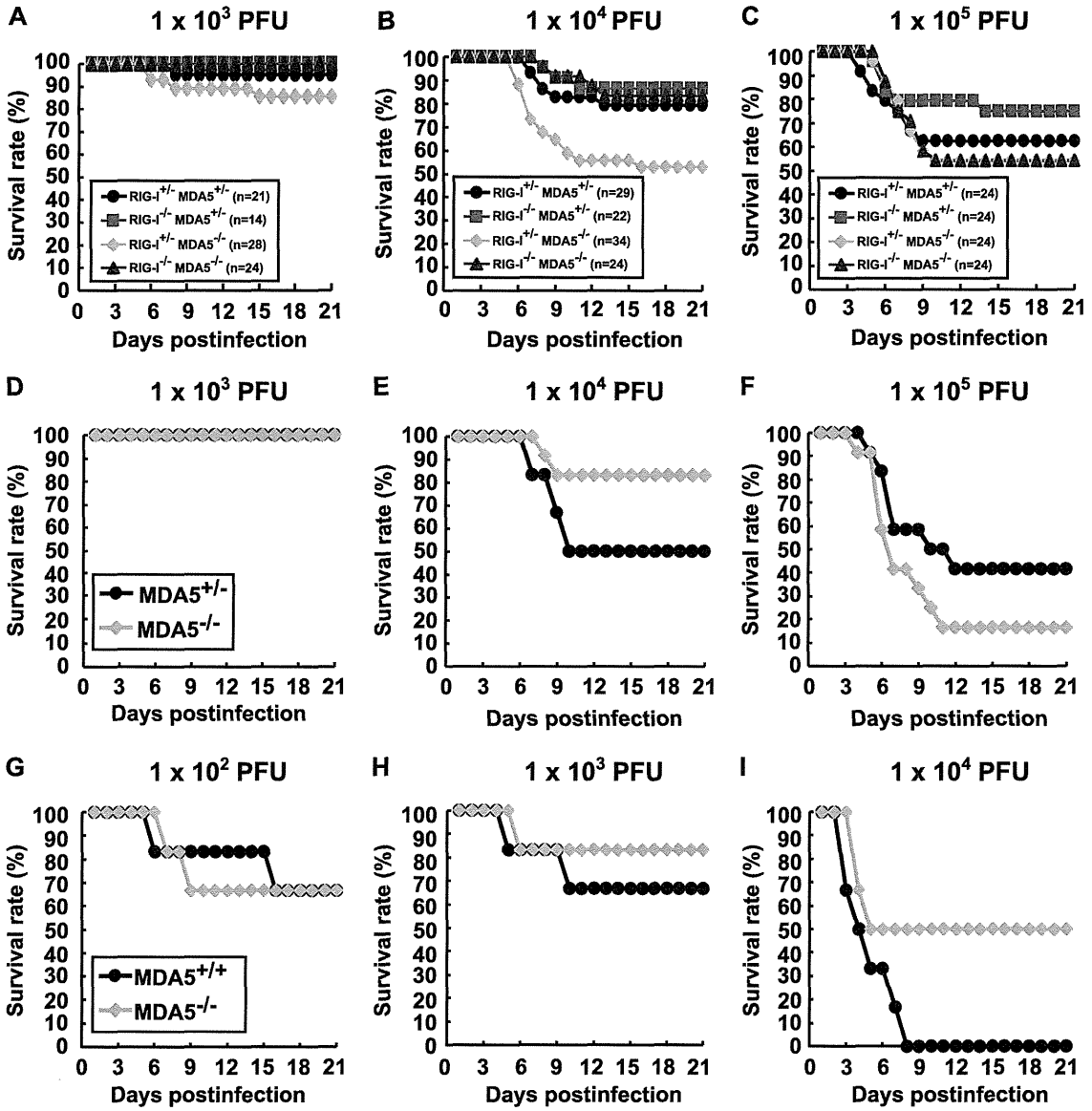

FIG 5 Mortality rates of RIG-I- and MDA5-deficient mice. Littermates of the genotypes indicated were obtained by mating RIGI-I$^{+/-}$ MDA5$^{+/-}$ and RIGI-I$^{-/-}$ MDA5$^{-/-}$ mice in the ICR background. The mice were infected intravenously with 10^3 (A), 10^4 (B), or 10^5 (C) PFU of PV. The results shown are the sums of several independent experiments. The total numbers of mice of the different genotypes that were used are boxed, and the doses used are shown at the top. Littermates of MDA5$^{+/-}$ and MDA5$^{-/-}$ mice were obtained in the B6 background. The mice (n = 12) were intravenously infected with 10^3 (D), 10^4 (E), or 10^5 (F) of PV. MDA5$^{+/+}$ and MDA5$^{-/-}$ mice (n = 6) were intracerebrally infected with 10^2 (G), 10^3 (H), or 10^4 (I) PFU of PV, respectively. We monitored the survival rates of the mice for 3 weeks after infection.

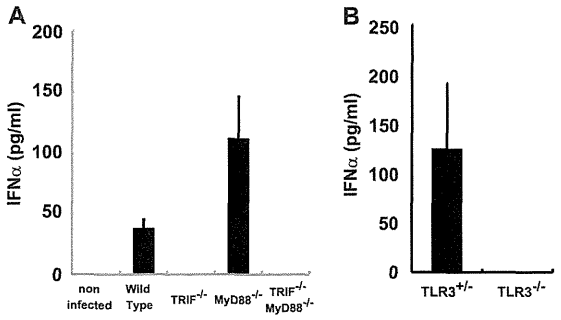

FIG 6 Production of serum IFN-α in TRIF-, MyD88-, and TLR3-deficient mice. Mice (n = 3 or 8) were intravenously infected with 10^7 PFU of PV. IFN-α levels of TRIF- and MyD88-deficient mice (A) and TLR3-deficient mice (B) at 12 hpi were compared. The experiments were repeated twice, and representative data are shown.

were inoculated with 10^4 PFU of PV. We suspect that the slight difference between the mortality rates of wild-type and MDA5$^{-/-}$ mice was in the range of experimental fluctuation, and thus, the disruption of MDA5 did not significantly influence the mortality rate. In order to determine if the same is true when mice are infected by other routes, we inoculated wild-type and MDA5$^{-/-}$ mice with PV intracerebrally and compared their mortality rates (Fig. 5G to I). Their mortality rates did not differ significantly. These results suggest that MDA5 does not make a great contribution to the protection of mice, at least after intracerebral and intravenous infections. Taken together, the MDA5-mediated response does not play a dominant role in IFN production, ISG induction, or inhibition of PV replication *in vivo*, unlike the MDA5-mediated effects on EMCV infection.

IFN response in TRIF- and MyD88-deficient mice. Because the experiments with MDA5-deficient mice suggested the existence of other protective mechanisms in PV infection, we investigated the role of TLRs using TRIF- and MyD88-deficient mice. PVR-tg mice were mated with TRIF$^{-/-}$ and/or MyD88$^{-/-}$ mice in the B6 background. Serum IFN-α of mice infected with 10^7 PFU of PV was measured using ELISA at 12 hpi (Fig. 6A). Interestingly, serum IFN production in response to PV infection was abrogated in TRIF$^{-/-}$ mice. Because TRIF acts as an adaptor for TLR3 and TLR4, we tested whether the same phenomenon occurs in TLR3$^{-/-}$ mice. Serum IFN induction was not observed in TLR3-deficient mice (Fig. 6B). These results suggest that the TLR3-mediated pathway is essential for IFN production in response to PV infection.

We next assessed the induction of mRNAs for OAS1a (Fig. 7A) and IRF-7 (Fig. 7B) in various organs using real-time RT-PCR. The induction of OAS1a and IRF-7 was observed in all mice. Although serum IFN production was abrogated in TRIF$^{-/-}$ mice and TRIF$^{-/-}$ MyD88$^{-/-}$ mice (Fig. 6), a significant level of ISG mRNA was induced. However, the induction levels were slightly lower than those in wild-type mice in some cases. The results suggest that the TRIF-mediated pathway contributes to ISG expression mainly through the induction of serum IFNs in response to PV infection and that some other mechanisms may also contribute to ISG expression.

PV replication in nonneural tissues and mortality rates of TRIF- and MyD88-deficient mice. The brain, spinal cord, liver, spleen, and kidney of paralyzed mice were recovered, and viral titers were determined (Fig. 8). PV was recovered from the CNS of TRIF$^{-/-}$, MyD88$^{-/-}$, and TLR3$^{-/-}$ mice, and the titers were not different from those of wild-type mice. However, the viral titers of the liver, spleen, and kidney of TRIF$^{-/-}$ and TLR3$^{-/-}$ mice were significantly higher than those of wild-type mice but lower than those of IFNAR1$^{-/-}$ mice. We then examined the virus replication kinetics in TRIF$^{-/-}$ mice (Fig. 8B). The viral load in the CNS increased in TRIF$^{-/-}$ mice similarly to that in other mice. In accordance to the absence of serum IFN (Fig. 2), the viral loads in the liver, spleen, and kidney of TRIF$^{-/-}$ mice increased, while the viral loads in these organs of wild-type mice decreased. PV antigens were detected in the CNS of all of the knockout mice. In addition, PV antigens were detected in the adipose tissue, pancreas, and kidney of several TRIF$^{-/-}$ and MyD88$^{-/-}$ mice (Table 2). These results suggest that these tissues support viral multiplication in these knockout mice and that the TLR-mediated signaling pathways contribute to the regulation of PV replication in nonneural tissues.

The mortality rates of TRIF$^{-/-}$, MyD88$^{-/-}$, and TLR3$^{-/-}$

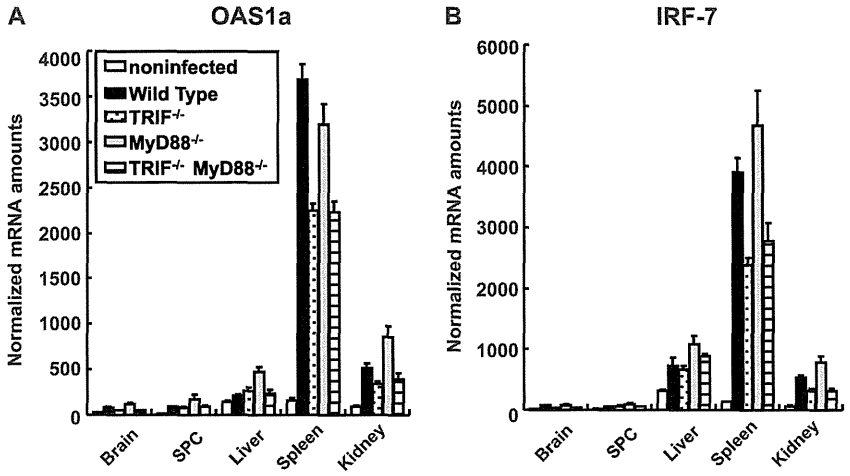

FIG 7 ISG induction in TRIF- and MyD88-deficient mice. Mice (n = 4) were intravenously infected with 10^7 PFU of PV. At 12 hpi, RNA was isolated from the indicated tissues of the infected mice and OAS1a (A) and IRF-7 (B) mRNA levels were determined by quantitative real-time PCR. The experiments were repeated twice, and representative data are shown. SPC, spinal cord.

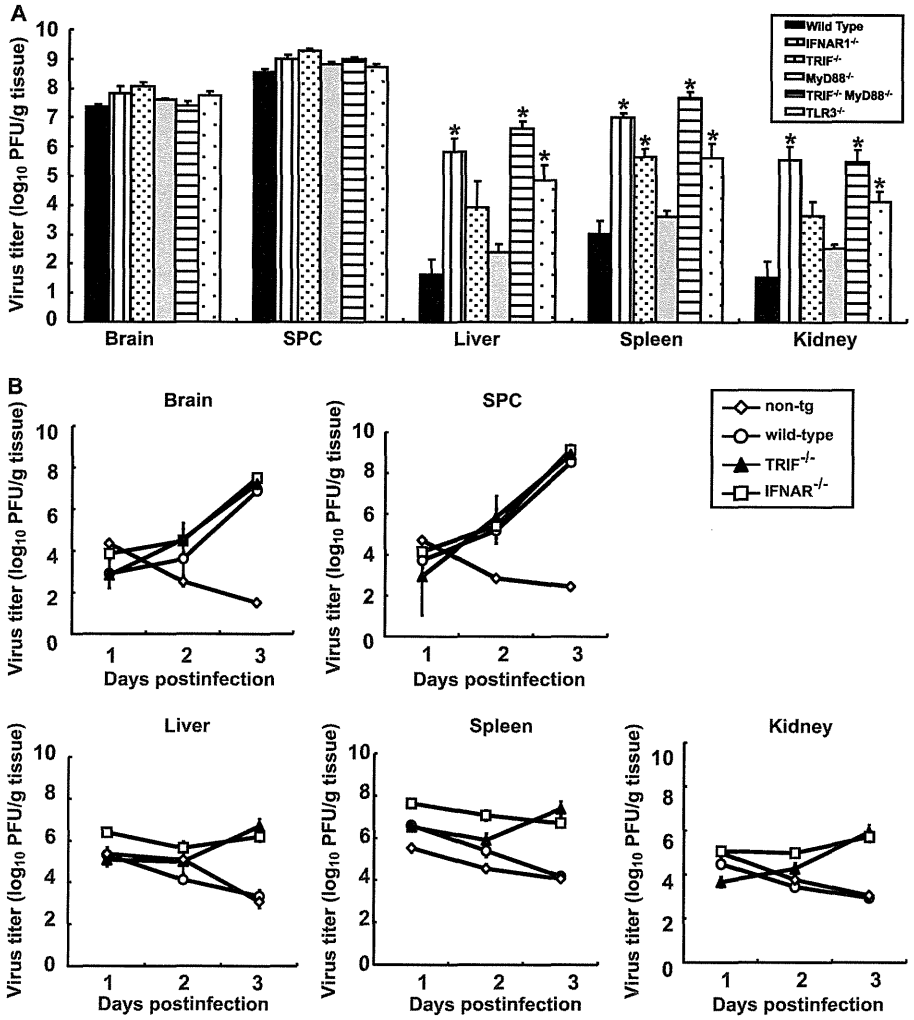

FIG 8 (A) PV replication in TRIF- and MyD88-deficient mice. Wild-type ($n = 4$), TRIF$^{-/-}$ ($n = 4$), MyD88$^{-/-}$ ($n = 6$), TRIF$^{-/-}$ MyD88$^{-/-}$ ($n = 4$), TLR3$^{-/-}$ ($n = 5$), and IFNAR1$^{-/-}$ ($n = 4$) mice were intravenously infected with 10^7 PFU of PV. The infected mice were paralyzed or dead at 3 to 5 days postinfection. The indicated tissues were collected, and viral titers were determined using a plaque assay (*, $P < 0.01$ by t test compared to wild-type mice). (B) PV replication kinetics in TRIF-deficient mice. Nontransgenic mice, wild-type mice, TRIF$^{-/-}$ mice, and IFNAR1$^{-/-}$ mice ($n = 3$) were infected as described above. Tissues were collected daily, and viral titers were determined. The results for nontransgenic (non-tg) mice, wild-type mice, and IFNAR1$^{-/-}$ mice are the same as those in Fig. 4B. SPC, spinal cord.

TABLE 2 PV antigens in TRIF- and MyD88-deficient mice

Organ or tissue	No. of PV antigen-positive mice/no. of mice tested			
	Wild type	TRIF$^{-/-}$	MyD88$^{-/-}$	TRIF$^{-/-}$ MyD88$^{-/-}$
Brain	6/6	8/8	9/9	6/6
Spinal cord	6/6	8/8	9/9	6/6
Heart	0/6	0/8	0/8	0/6
Lung	0/6	0/8	0/8	0/6
Liver	0/6	0/8	0/9	0/6
Kidney	0/6	0/8	2/9	0/5
Spleen	0/6	0/8	0/9	0/6
Pancreas	2/6	0/8	7/9	4/6
Intestine	0/6	0/8	0/9	0/6
Adipose tissue	0/6	2/8	2/9	3/6

mice were compared (Fig. 9). Approximately 25% of the TRIF$^{-/-}$ mice died after infection with 10^2 PFU of PV, and almost all of the mice died after infection with more than 10^3 PFU of PV (Fig. 9A). Approximately 20% and 60% of the MyD88$^{-/-}$ mice died after infection with 10^3 and 10^4 PFU of PV, respectively (Fig. 9B and C). TRIF$^{-/-}$ MyD88$^{-/-}$ mice were the most susceptible. In total, 70% of the mice died after infection with 10^2 PFU of PV (Fig. 9A). The mortality rate of TRIF$^{-/-}$ MyD88$^{-/-}$ mice was very close to that of IFNAR1$^{-/-}$ mice (19). The mortality rate of TLR3$^{-/-}$ mice was similar to that of TRIF$^{-/-}$ mice (Fig. 9D, E, and F). These results suggest that the TRIF-mediated and MyD88-mediated antiviral responses contribute to the host's defense against PV infection and that the TLR3-TRIF-mediated response has the most dominant effect.

DISCUSSION

Each virus infects different cell types and has a characteristic mode of replication. In mammalian hosts, several viral RNA sensors,

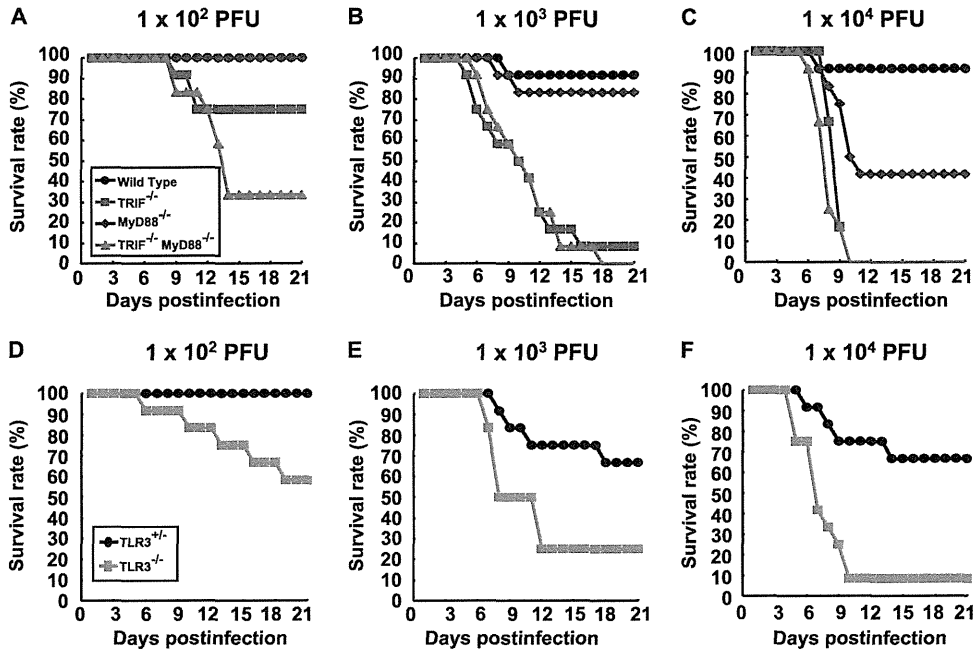

FIG 9 Mortality rates of TRIF-, MyD88-, and TLR3-deficient mice. (A) Wild-type, TRIF$^{-/-}$, MyD88$^{-/-}$, and TRIF$^{-/-}$ MyD88$^{-/-}$ mice (n = 12) were intravenously inoculated with the indicated doses of PV. (B) Littermates of TLR3$^{+/-}$ and TLR3$^{-/-}$ mice (n = 12) were used.

which are expressed in different cell types and recognize different molecular patterns, have evolved to counteract a variety of viruses. In the present study, we demonstrated that the MDA5-, TRIF-, and MyD88-mediated pathways contribute to the recognition of PV infection and that the TLR3-TRIF-mediated pathway plays the most important role in the antiviral response. Since all of the phenotypes shown after PV infection in the TRIF$^{-/-}$ mice and TLR3$^{-/-}$ mice are very similar to each other, we think that the contribution of the TLR3-mediated response is dominant and that of the TLR4-mediated response is negligible.

Previous reports have revealed that IFN is produced efficiently in EMCV-infected fibroblasts in an MDA5-dependent manner and that MDA5 contributes to the induction of serum IFNs and the protection of mice against EMCV (10, 23). Because EMCV belongs to the family *Picornaviridae*, we hypothesized that MDA5 also contributes to IFN induction in response to PV infection. However, the MDA5-dependent pathway did not play a dominant role in the defense against PV infection. Therefore, we speculate that PV uses mechanisms different from those of EMCV to strongly suppress IFN production *in vivo*. Indeed, IFN production in cultured cells in response to PV infection was observed only when the cells were pretreated with a low dose of IFNs. In addition, the amount of IFN produced was much lower than that produced in response to EMCV infection (Fig. 1). This result suggests that IFN induction in infected cells is suppressed and that this PV-mediated effect may be stronger than that of EMCV. Translational shutoff may be one of the reasons for this difference. PV 3A protein causes a change in membrane trafficking that prevents protein secretion and may also contribute to the suppression of IFN production (6). Caspase-dependent cleavage of MDA5 (3) and IPS-1 (39) in PV-infected cells has been reported. Through these possible mechanisms, PV may induce the suppression of IFN production in mice *in vivo*, and the MDA5-mediated pathway does not play an essential role in the host response, unlike in EMCV infection. PV and EMCV seemed to use different strategies to counteract the host innate immune system, even though PV and EMCV belong to the same family. Thus, TLR3 became the sensor that functions most effectively for PV as a result of PV evolution. Although the TLR3-TRIF-mediated pathway plays a dominant role, the fact that significant ISG induction was observed in PV-infected TRIF$^{-/-}$ and TRIF$^{-/-}$ MyD88$^{-/-}$ mice (Fig. 7) suggested that other mechanisms also operate in combination with this pathway.

The viral loads in the nonneural tissues of TLR3- and TRIF-deficient mice were much higher than those in wild-type mice, whereas the viral loads in the CNS were not significantly different in paralyzed mice (Fig. 8). These results suggest that the TLR3-TRIF-mediated pathway inhibits viral replication mainly before viral invasion of the CNS rather than after invasion and that this response plays an important role in preventing the viral invasion of the CNS. In the CNS, replication of PV was not effectively inhibited, even in wild-type mice. This result is consistent with our previous results obtained using IFNAR1$^{-/-}$ mice and suggests that the antivirus response in the CNS is different from that in nonneural tissues upon PV infection (19). The cell tropism of PV may influence the efficiency of the immune response. For example, if PVR is expressed in TLR3-expressing cells, then PV replication would be detected immediately after infection. Alternatively, if PV infection *in vivo* occurs in the vicinity of TLR3-expressing immune cells such as DCs and macrophages, PV-infected cells may readily be captured by TLR3-expressing cells, thereby facilitating efficient cross-priming (27, 44) of PV RNA. PV infects neurons almost exclusively and not other cell types in the CNS. If neurons do not have the ability to induce a strong TLR3-mediated antiviral response upon PV infection, the CNS may be more defective in the innate immune response than nonneural tissues are. This may be one of the reasons why PV replicates preferentially in the CNS. Further studies on PV pathogenesis related to the innate

immune response will make a great contribution to elucidating the mechanisms of PV tissue tropism.

TLR3 recognizes dsRNA. However, the protective role of TLR3 in the response to many RNA viral infections is not clear (9, 29, 43). A previous study has demonstrated that WNV, which is an encephalitis virus belonging to the family *Flaviviridae*, causes more severe encephalitis in mice with intact TLR3 than in TLR3$^{-/-}$ mice. Peripheral WNV infection leads to a breakdown of the blood-brain barrier (BBB) and enhances brain infection in wild-type mice but not in TLR3$^{-/-}$ mice (50). In contrast, a protective role of the TLR3-mediated pathway in PV infection was clearly demonstrated in the present study. PV enters the CNS directly across the BBB via a PVR-independent mechanism (52) and from the neuromuscular junction via retrograde axonal transport (31–33). Because PV originally possesses two entry pathways into the CNS, the generation of a new entry pathway, even if it did occur, might not increase its deteriorative effect.

Interestingly, protective roles of the TLR3-mediated pathway have been reported for group B coxsackievirus (30, 41, 42), human rhinovirus (49), and EMCV (11) infections. Riad et al. (41) demonstrated that TRIF$^{-/-}$ mice showed severe myocarditis after CVB3 infection and IFN-β treatment improved virus control and reduced cardiac inflammation. Richer et al. (42) reported that TLR3$^{-/-}$ mice produced reduced proinflammatory mediators and were unable to control CVB4 replication at the early stages of infection, resulting in severe cardiac damage. They also showed that adoptive transfer of wild-type macrophages into TLR3$^{-/-}$ mice challenged with CVB4 resulted in greater survival, suggesting the importance of the TLR3-mediated pathway in the macrophage. Negishi et al. (30) reported that TLR3$^{-/-}$ mice showed vulnerability to CVB3 and that TLR3 signaling is linked to the activation of the type II IFN system. Since CVB3 does not induce robust type I IFNs, they suggested that the TLR3 type II IFN pathway serves as an "ace in the hole" in infections with such viruses. PV is similar to CVB3 because type I IFN production is low. However, in our preliminary experiments on PV infection in IFN-$\gamma^{-/-}$ PVR-tg mice, type II IFN did not make a significant contribution to the pathogenesis of PV. Taken together, these results suggest a critical role for the TLR3-mediated pathway, but the precise mechanisms leading to host protection are still controversial and the downstream events of TLR3 signaling after picornavirus infection remain to be elucidated.

Because the above-mentioned viruses are picornaviruses, picornavirus RNA may be easily detected by TLR3. There may be a common RNA structure in the genome or in the replication intermediates of these viruses that is detected by TLR3. Alternatively, picornaviral RNA may replicate in a compartment in which TLR3 can easily access the replicating dsRNA. To investigate these hypotheses, identification of the cells responsible for IFN production is an important step. Oshiumi et al. demonstrated that splenic CD8α^+ CD11c$^+$ cells, bone marrow-derived macrophages, and DCs are able to elicit IFN in response to PV infection (35). Further studies using this virus-cell system will elucidate the molecular recognition pattern in the PV genome, the precise mechanism of PV RNA recognition in TLR3-expressing cells, and the roles of these cells in the prevention of PV dissemination in the body.

ACKNOWLEDGMENTS

We thank Takashi Fujita, Mitsutoshi Yoneyama, Hiroki Kato, Masahiro Yamamoto, Satoshi Uematsu, Seiya Yamayoshi, Akira Ainai, Hideki Hasegawa, and Takashi Kawanishi for helpful discussions and technical assistance.

This work was supported, in part, by Grants-in-Aid from the Ministry of Education, Culture, Sports, Science and Technology, Japan (Grants-in-Aid for Scientific Research on Priority Areas no. 21022053), and Grants-in-Aid for Research on Emerging and Re-emerging Infectious Diseases from the Ministry of Health, Labor and Welfare, Japan.

REFERENCES

1. **Akira S, Uematsu S, Takeuchi O.** 2006. Pathogen recognition and innate immunity. Cell **124**:783–801.
2. **Alexopoulou L, Holt AC, Medzhitov R, Flavell RA.** 2001. Recognition of double-stranded RNA and activation of NF-kappaB by Toll-like receptor 3. Nature **413**:732–738.
3. **Barral PM, et al.** 2007. MDA-5 is cleaved in poliovirus-infected cells. J. Virol. **81**:3677–3684.
4. **Bodian D.** 1959. Poliomyelitis: pathogenesis and histopathology, p 479–518. *In*Rivers TM, Horsfall FL, Jr (ed), Viral and rickettsial infections of man, vol 3. J. B. Lippincott, Philadelphia, PA.
5. **Cella M, et al.** 1999. Plasmacytoid monocytes migrate to inflamed lymph nodes and produce large amounts of type I interferon. Nat. Med. **5**:919–923.
6. **Choe SS, Dodd DA, Kirkegaard K.** 2005. Inhibition of cellular protein secretion by picornaviral 3A proteins. Virology **337**:18–29.
7. **Colonna M, Trinchieri G, Liu YJ.** 2004. Plasmacytoid dendritic cells in immunity. Nat. Immunol. **5**:1219–1226.
8. **Diebold SS, Kaisho T, Hemmi H, Akira S, Reis e Sousa C.** 2004. Innate antiviral responses by means of TLR7-mediated recognition of single-stranded RNA. Science **303**:1529–1531.
9. **Edelmann KH, et al.** 2004. Does Toll-like receptor 3 play a biological role in virus infections? Virology **322**:231–238.
10. **Gitlin L, et al.** 2006. Essential role of mda-5 in type I IFN responses to polyriboinosinic:polyribocytidylic acid and encephalomyocarditis picornavirus. Proc. Natl. Acad. Sci. U. S. A. **103**:8459–8464.
11. **Hardarson HS, et al.** 2007. Toll-like receptor 3 is an essential component of the innate stress response in virus-induced cardiac injury. Am. J. Physiol. Heart Circ. Physiol. **292**:H251–H258.
12. **Hemmi H, et al.** 2002. Small anti-viral compounds activate immune cells via the TLR7 MyD88-dependent signaling pathway. Nat. Immunol. **3**:196–200.
13. **Hoebe K, et al.** 2003. Identification of Lps2 as a key transducer of MyD88-independent TIR signalling. Nature **424**:743–748.
14. **Holland JJ.** 1961. Receptor affinities as major determinants of enterovirus tissue tropisms in humans. Virology **15**:312–326.
15. **Holland JJ, Mc LL, Syverton JT.** 1959. Mammalian cell-virus relationship. III. Poliovirus production by non-primate cells exposed to poliovirus ribonucleic acid. Proc. Soc. Exp. Biol. Med. **100**:843–845.
16. **Holland JJ, McLaren LC, Syverton JT.** 1959. The mammalian cell-virus relationship. IV. Infection of naturally insusceptible cells with enterovirus ribonucleic acid. J. Exp. Med. **110**:65–80.
17. **Hornung V, et al.** 2006. 5′-Triphosphate RNA is the ligand for RIG-I. Science **314**:994–997.
18. **Hsiung GD, Black FL, Henderson JR.** 1964. Susceptibility of primates to viruses in relation to taxonomic classification, p 1–23. *In*Buettner-Jaenusch J (ed), Evolutionary and genetic biology of primates, vol 2. Academic Press, New York, NY.
19. **Ida-Hosonuma M, et al.** 2005. The alpha/beta interferon response controls tissue tropism and pathogenicity of poliovirus. J. Virol. **79**: 4460–4469.
20. **Ida-Hosonuma M, et al.** 2003. Host range of poliovirus is restricted to simians because of a rapid sequence change of the poliovirus receptor gene during evolution. Arch. Virol. **148**:29–44.
21. **Kato H, et al.** 2005. Cell type-specific involvement of RIG-I in antiviral response. Immunity **23**:19–28.
22. **Kato H, et al.** 2008. Length-dependent recognition of double-stranded ribonucleic acids by retinoic acid-inducible gene-I and melanoma differentiation-associated gene 5. J. Exp. Med. **205**:1601–1610.
23. **Kato H, et al.** 2006. Differential roles of MDA5 and RIG-I helicases in the recognition of RNA viruses. Nature **441**:101–105.
24. **Koike S, et al.** 1992. A second gene for the African green monkey poliovirus receptor that has no putative N-glycosylation site in the functional N-terminal immunoglobulin-like domain. J. Virol. **66**:7059–7066.